Alba, Vincenzo, et al. Unusual area-law violation in random inhomogeneous systems. *Journal of Statistical Mechanics: Theory and Experiment*, (Feb. 2019) 023105, pp. 1-43.

DOI: https://doi.org/10.1088/1742-5468/ab02df

Unusual area-law violation in random inhomogeneous systems

Vincenzo Alba[1,6], Silvia N Santalla[2], Paola Ruggiero[1], Javier Rodriguez-Laguna[3], Pasquale Calabrese[1,4] and German Sierra[5]

[1] International School for Advanced Studies (SISSA) and INFN, Via Bonomea 265, 34136, Trieste, Italy
[2] Departamento de Física and Grupo Interdisciplinar de Sistemas Complejos (GISC), Universidad Carlos III de Madrid, Leganés, Spain
[3] Departamento de Física Fundamental, Universidad Nacional de Educacion a Distancia (UNED), Madrid, Spain
[4] International Centre for Theoretical Physics (ICTP), 34151, Trieste, Italy
[5] Instituto de Física Teórica UAM/CSIC, Universidad Autónoma de Madrid, Madrid, Spain

Abstract. The discovery of novel entanglement patterns in quantum many-body systems is a prominent research direction in contemporary physics. Here we provide the example of a spin chain with random and inhomogeneous couplings that in the ground state exhibits a very unusual area-law violation. In the clean limit, i.e. without disorder, the model is the rainbow chain and has volume law entanglement. We show that, in the presence of disorder, the entanglement entropy exhibits a power-law growth with the subsystem size, with an exponent 1/2. By employing the strong disorder renormalization group (SDRG) framework, we show that this exponent is related to the survival probability of certain random walks. The ground state of the model exhibits extended regions of short-range singlets (that we term 'bubble' regions) as well as rare long range singlet ('rainbow' regions). Crucially, while the probability of extended rainbow regions decays exponentially with their size, that of the bubble regions is power law. We provide strong numerical evidence for the correctness of SDRG results by exploiting the free-fermion solution of the

model. Finally, we investigate the role of interactions by considering the random inhomogeneous XXZ spin chain. Within the SDRG framework and in the strong inhomogeneous limit, we show that the above area-law violation takes place only at the free-fermion point of phase diagram. This point divides two extended regions, which exhibit volume-law and area-law entanglement, respectively.

Keywords: disordered spin chains, entanglement entropies, entanglement in extended quantum systems, spin chains, ladders and planes

Contents

1. Introduction **3**

2. The random inhomogeneous XX chain (randbow chain) **5**
2.1. Strong disorder renormalization group (SDRG) method 8
2.2. Path invariance of the SDRG for the XX chain: a useful lemma 9
2.3. Entanglement entropy of random singlet states 11

3. Area-law violation in the random inhomogeneous XX chain **12**
3.1. Von Neumann entropy: SDRG results 12
3.2. Understanding the area-law violation: bubble versus rainbow regions 13

4. Entanglement contour **16**

5. Numerical benchmarks using the exact solution of the XX chain **19**

6. Energy gap **21**

7. A toy model for the strongly inhomogeneous limit **23**
7.1. Rainbow diagrams: random walk and survival probability 24
7.2. Bubble diagrams: random walk and survival probability 25

8. Entanglement entropy in the interacting case **26**
8.1. Random walk interpretation 28

9. Conclusions **29**
Acknowledgments **30**
Appendix A. SDRG and ternary algebras **30**
Appendix B. Survival probabilities: exact results **32**
B.1. Rainbow diagram 32
B.2. Bubble diagram 37
B.3. Asymptotic behavior of the length of the bubble diagrams 38
Appendix C. Random walk survival probabilities: numerical simulations **39**

References **40**

1. Introduction

A striking feature of local gapped quantum many-body systems is that the ground-state entanglement entropy of a subsystem scales with the area of its boundary rather than with its volume [1–4]. This statement is the essence of the famous *area law* for the entanglement. Given a quantum system in a pure state in D dimensions, and given a bipartition of the system into a subsystem A and its complement $\bar{A}$ (see, for instance, figure 1 for a one-dimensional setup), the von Neumann entanglement entropy is defined as

$$S \equiv -\mathrm{Tr}\rho_A \ln \rho_A, \tag{1}$$

where ρ_A is the reduced density matrix of A, which is obtained by tracing over the degrees of freedom of $\bar{A}$ in the full-system density matrix ρ. After denoting as ℓ the typical length of A, the area law states that for large ℓ the entanglement entropy scales like $S \propto \ell^{D-1}$. Physically, the area law suggests that the ground state of local Hamiltonians contains much less quantum correlation than what one might have expected. The area law has enormous consequences for the simulability of quantum states using classical computers. For instance, it underlies the extraordinary success of Matrix Product States (MPS) methods, such as the Density Matrix Renormalization Group [5–7] (DMRG) to effectively describe ground states of one-dimensional systems. For gapped many-body systems, there is an unanimous consensus that the area law is valid in arbitrary dimension [1], although a rigorous proof is only available for one-dimensional systems [8] (see also [9]). Conversely, it is well known that the ground states of gapless free-fermionic Hamiltonians exhibit logarithmic corrections to the area law [10–12], i.e. one has $S = \mathcal{O}(\ell^{D-1} \ln \ell)$, in contrast with gapless bosonic systems [13], for which no corrections are present for $d \geqslant 2$. However, the most prominent examples of logarithmic area-law violations are critical one-dimensional models whose low energy properties are captured by a conformal field theory (CFT) [14–17], and spin chains with a permutation symmetric ground state [18–21]. Importantly, the area-law is not generic. *Typical* excited states of local Hamiltonians exhibit a volume law entanglement [22–24] (and in these cases the density of entanglement entropy is the same as the thermodynamic entropy of a generalised microcanonical ensemble at the correct energy, see, e.g. [25]). However, there are many examples of eigenstates with sub-volume (logarithmic) scaling of the entanglement entropy (see, e.g. [24, 26]), in particular when the low-energy part of the spectrum is described by a CFT for which exact analytic predictions are obtainable [27–35].

Motivated by this evidence, there is strong common belief that ground states of 'physically reasonable local Hamiltonians' fulfil the area law, and that violations are at most logarithmic (see, however, [36]). Only very recently, devising local models that exhibit more dramatic area-law violations became an important research theme. The motivation is twofold. On the one hand, highly-entangled ground states are potentially useful for quantum computation technologies. On the other hand, from a condensed matter perspective, area-law violations could be witnesses of exotic features of quantum matter. As a matter of fact, examples of ground states violating the area law start to be discovered (see, for instance, [37–51]). These comprise inhomogeneous systems [39], translation invariant models with large spin [37], free-fermion Hamiltonians [43] with

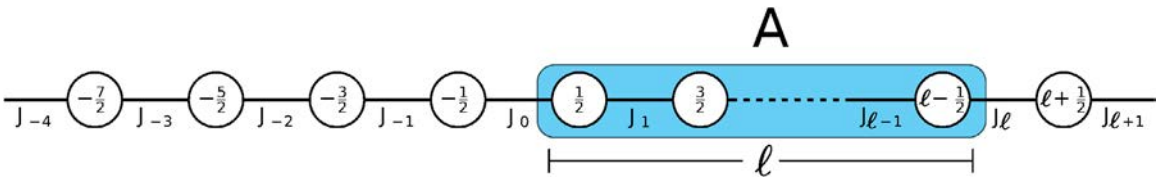

Figure 1. Setup used in this work. (Top) definition of the random inhomogeneous XX chain. The chain couplings are denoted as $J_n = \mathrm{e}^{-|n|h} K_n$, with n half integer numbers, h a real inhomogeneity parameter, and K_n independent random variables distributed with (4). In this work we focus on the entanglement entropy of a subregion A of length ℓ (shaded area in the figure). Subsystem A starts from the chain center.

a fractal Fermi surface, nonlocal quantum field theories [42], and supersymmetric models [41]. An interesting class of frustration-free, local, translational invariant models that exhibit area-law violations has been constructed by Movassagh and Shor in [44]. Their ground-state entanglement entropy is $\propto \ell^{1/2}$, thus exhibiting a polynomial violation of the area law. Importantly, the exponent of the entanglement growth originates from universal properties of the random walk. This is due to the fact that the ground state of the model is written in terms of a special class of combinatorial objects, called Motzkin paths [52]. A similar result can be obtained [45, 46] using the Fredkin gates [53]. An interesting generalization of [44] obtained by deforming a colored version of the Motzkin paths has been presented in [47]. The ground-state phase diagram of the model exhibits two phases with area-law and volume-law entanglement, respectively. These are separated by a 'special' point, where the ground state displays square-root entanglement scaling.

In this paper, we show that unusual area-law violations can be obtained in a one-dimensional inhomogeneous local system in the presence of disorder. Specifically, here we investigate the random inhomogeneous XX chain. In the clean limit, i.e. in the absence of disorder, our model reduces to the rainbow chain of [39], whose ground state, in the limit of strong inhomogeneity, is the rainbow state. In the rainbow state long-range singlets are formed between spins across the chain center. An immediate striking consequence is that the half-chain entanglement entropy is proportional to the subsystem volume (volume law). Here we show that upon including disorder the structure of the ground state changes dramatically. In contrast with the clean case, now the probability of having long-range singlets across the chain center is strongly suppressed. In particular, the probability of having extended regions (that we term 'rainbow' regions) of mirror symmetric singlets across the chain center decays exponentially with the region size. On the other hand, the probability of having extended regions with short-range singlets connecting nearest-neighbor spins decays algebraically with the region size, with an exponent 3/2. This has striking consequences for the entanglement scaling. Precisely, in contrast with the clean case, the entropy exhibits an unusual square root growth, which represents a polynomial violation of the area law. We provide numerical evidence for this behavior by using the strong disorder renormalization group (SDRG) method [54] (see also [55]). We numerically verify that the unusual area-law violation happens both in the strong inhomogeneous limit, as well as for weak inhomogeneity. Specifically, we numerically observe the square-root scaling for considerably weak inhomogeneity, although we do not have any proof that it

persists for arbitrarily small one. We provide robust numerical evidence of the unusual area-law violation in a microscopic model by calculating the entanglement entropy of the random inhomogeneous XX chain, which is obtained by using the free-fermion solution of the model. Furthermore, we establish a mapping between the SDRG flow of the renormalized couplings and an alternating random walk. Interestingly, in the strong inhomogeneous limit the exponents of the entanglement scaling, and several ground-state features, can be quantitatively understood from certain survival probabilities of the random walk. Finally, we investigate the role of interactions by considering the random inhomogeneous spin-1/2 XXZ chain. Within the SDRG framework, we show that the unusual area-law violation does not survive in the presence of interactions. Precisely, we find that the entanglement entropy exhibits square-root scaling only at the XX point. Interestingly, this marks the transition between two extended regions, where the entanglement entropy exhibits area-law and volume-law scaling, respectively. Both the two behaviors can be qualitatively understood in the SDRG framework by exploiting the mapping to the random walk, at least in the strong inhomogeneous limit. This scenario is somewhat similar to the one presented in [47], although the models are substantially different.

The paper is organized as follows. In section 2 we introduce the random inhomogeneous XX chain and the SDRG framework. In particular, in section 2.2 we show that for the XX chain the SDRG renormalization flow exhibits an intriguing independence on the specific renormalization pattern. In section 3 we present numerical SDRG results for the entanglement entropy in the XX chain. In section 4 we describe how the unusual area-law violation is reflected in the behavior of the entanglement contour. In section 5, by exploiting the exact solvability of the random inhomogeneous XX chain, we provide evidence of the area-law violation. In section 6 we discuss the scaling of the energy gap. In section 7 we address the strongly inhomogeneous limit of the model, by exploiting a mapping between the SDRG flow and the random walk. Section 8 is devoted to discuss the entanglement scaling in the XXZ chain. We conclude in section 9. Finally, in appendix A we propose an algebraic interpretation of the SDRG scheme, and in appendix B we report the calculations of certain survival probabilities for the random walk introduced in section 7.

2. The random inhomogeneous XX chain (randbow chain)

We consider a chain with $2L$ sites, described by the following inhomogeneous random hopping Hamiltonian (see figure 1)

$$H = -\frac{1}{2}\sum_{m=-L+1}^{L-1} J_m \, c^\dagger_{m-\frac{1}{2}} c_{m+\frac{1}{2}} + \text{h.c.}, \quad \text{with } m = 0, \pm 1, \pm 2, \cdots, \pm(L-1). \tag{2}$$

Here $c_{m\pm\frac{1}{2}}$ ($c^\dagger_{m\pm\frac{1}{2}}$) denotes the annihilation (creation) operator of a spinless fermion at sites $m \pm \frac{1}{2}$, and $J_m > 0$ is the inhomogeneous random hopping parameter between the sites $m - \frac{1}{2}$ and $m + \frac{1}{2}$. In (2), the coupling J_0 is associated to the link $\left(-\frac{1}{2}, \frac{1}{2}\right)$ located at the center of the chain. The hopping parameters J_m are defined as

$$J_m \equiv K_m \times \begin{cases} \mathrm{e}^{-h/2}, & m = 0\,, \\ \mathrm{e}^{-h|m|}, & |m| > 0\,, \end{cases} \tag{3}$$

where $h > 0$ is a real parameter that measures the strength of the inhomogeneity. If $K_m = \mathcal{O}(1)$ are nonzero, for $h > 0$ the coupling strength decreases exponentially with the distance from the chain center. In (3), we choose K_m to be independent (from site to site) random variables distributed in the interval $[0, 1]$ according to

$$P(K) = \delta^{-1} K^{-1+\frac{1}{\delta}}, \tag{4}$$

with $\delta > 0$ parametrizing the noise strength. For $\delta = 1$, $P(K)$ becomes the uniform distribution in the interval $[0, 1]$. For $\delta \to 0$, $P(K)$ is peaked at $K = 1$ and the model (2) is clean, i.e. without disorder. On the other hand, for $\delta \to \infty$, $P(K)$ is peaked at $K = 0$. In the limit $\delta \to \infty$, equation (4) defines the infinite randomness fixed point (IRFP) distribution, which describes the long-distance properties of the ground state of (2) for $h = 0$ and any δ (see below).

After a Jordan–Wigner transformation, the random hopping model in (2) is mapped onto the spin-1/2 inhomogeneous XX chain defined by

$$H = \frac{1}{2} \sum_{m=-L+1}^{L-1} J_m \, S^+_{m-\frac{1}{2}} S^-_{m+\frac{1}{2}} + \text{h.c.}, \quad \text{with } m = 0, \pm 1, \pm 2, \cdots, \pm(L-1)\,. \tag{5}$$

Here $S^\pm_m$ are spin-1/2 raising and lowering operators. In this work we investigate the ground-state entanglement entropy S of a subregion A that starts from the chain center. The precise bipartition that we consider is pictorially illustrated in figure 1.

Clearly, the properties of the model (5) depend on two parameters, h and δ, giving rise to a two-dimensional ground-state phase diagram. The clean homogeneous XX chain is recovered for $\delta \to 0$ and $h = 0$. Its ground state is critical, and it is described by a conformal field theory (CFT) with central charge $c = 1$. The entanglement entropy of a finite subsystem A exhibits a logarithmic area-law violation described by [17]

$$S = \frac{c}{3} \ln \ell + k, \tag{6}$$

with k a non-universal constant, ℓ the size of A, and $c = 1$ the central charge of the CFT. In this work we focus on the entanglement properties of (5) at $\delta > 0$. In the limit $h \to 0$ and for any finite δ (see (3)), equation (5) defines the random antiferromagnetic XX chain. The ground state of the model has been extensively studied using the SDRG [54, 56, 57], and it is described by the random singlet (RS) phase. The structure of the random singlet phase (RSP) is depicted in figure 2(a). In the figure the links denote a singlet bond between the spins at their end points. In the RS phase short bonds between spins on near neighbour sites are present, as well as bonds joining distant spins. A distinctive feature of the RS phase, which can be derived by using the SDRG approach, is that, similar to the clean case (see (6)), the entanglement entropy of a finite subregion scales logarithmically as [58–61]

$$S = \frac{\ln 2}{3} \ln \ell + k', \tag{7}$$

where k' is a non universal constant. The crucial difference with (6) is the $\ln 2$ prefactor. For the random XX chain, this prefactor can be interpreted as a renormalization of the central charge $c = 1$ due to the disorder, which reduces the amount of the entanglement (see, however, [62] for a counterexample).

For $\delta = 0$ and $h > 0$, the ground state of (5) is in the rainbow phase [39]. The structure of the ground state of (5) is illustrated in figure 2(c). The system exhibits a proliferation of long bonds connecting distant spins symmetrically across the chain center. This behavior can be understood in the strong inhomogeneity limit at $h \gg 1$, By using the SDRG method, one can easily show that the ground state of (5) is the *rainbow* state. In the language of fermions this reads

$$|\text{RAINBOW}\rangle = \prod_{n=1/2}^{L-1/2} \left(c^\dagger_{-n} + (-1)^{n-1/2} c^\dagger_{+n} \right) |0\rangle. \tag{8}$$

In the spin representation, the state (8) corresponds to a product of singlets between the sites $(-n, +n)$ of the chain. An important feature of the rainbow state (8) is that the entanglement entropy of a subsystem starting from the chain center grows linearly with its size ℓ (corresponding to a *volume* law) as [39, 63–67]

$$\lim_{h\to\infty} S(h, \ell) = \ell \ln 2, \tag{9}$$

where subleading $\mathcal{O}(1)$ terms have been neglected. Equation (9) reflects that the entanglement is proportional to the number of singlets shared between A and its complement $\bar{A}$, i.e. connecting a site in A and the other in $\bar{A}$. Remarkably, the volume-law scaling (9) survives in the weak inhomogeneity limit $h \to 0$. One can take the continuum limit of (2), by sending the lattice spacing $a \to 0$ and by considering $h \to 0$ and $L \to \infty$ with h/a and aL fixed, to show that the half-chain entanglement entropy is still linear with L, but with a different coefficient as [67]

$$S(h, L) \simeq \frac{1}{6} \ln \left(\frac{\mathrm{e}^{hL} - 1}{h} \right) \to \frac{hL}{6}. \tag{10}$$

The last expression in (10) is obtained in the limit $hL \gg 1$.

In this work we focus on the regime with finite nonzero δ and $0 < h < \infty$. In this regime the ground state of (5) is in a dramatically different phase. This is illustrated in figure 2(b). Its structure is easily understood in the limit $h \gg 1$. Similar to the rainbow phase, long bonds connecting spins on symmetric sites with respect to the center of the chain are present. However, in contrast with the rainbow case (see figure 2(c)), they are rare and do not form an extended phase. Precisely, the probability of forming a sequence of rainbow links decreases exponentially with its size, i.e. with the number of consecutive sites involved. On the other hand, the ground state of (5) exhibits a proliferation of short-range singlets between spins on nearest-neighbor sites. These form extended 'bubble' regions (see figure 2(b)). We anticipate that the probability of forming a bubble region of length ℓ_b decays as a power law as $\propto \ell_b^{-3/2}$, in contrast with that of forming a rainbow region, which is exponential. This has striking consequences for the scaling of the entanglement entropy. First, only rainbow bonds can contribute to the entanglement between A and the rest, because short singlets connect mostly sites within A and $\bar{A}$, separately. On the other hand, the typical length scale over which the

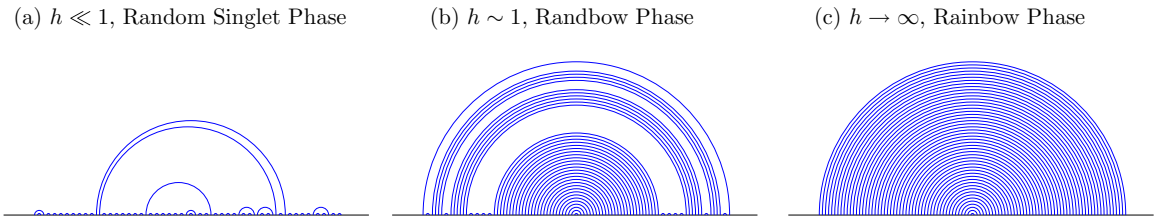

Figure 2. Summary of the phase diagram of the model, using open boundaries. Arcs in the figure correspond to spins forming $SU(2)$ singlet bonds. Notice that for any $h \neq 0$ the coupling strength J_i decreases exponentially away from the center of the chain. (a) For $h \ll 1$ the model becomes the XX chain with random antiferromagnetic couplings. The ground state of the model is the random singlet (RS) phase. In the RS phase bonds of arbitrary length are present, but no symmetry with respect to the chain center is observed. RS phases exhibit logarithmic entanglement growth. (b) For intermediate values of h we observe some long distance bonds along with a proliferation of short ones, connecting neighboring sites (bubbles). The bond diagram presents left-right symmetry, and the entanglement is characterized by a subextensive (square root) entanglement growth. (c) For $h \to \infty$ the model approaches the standard rainbow chain, with all bonds symmetric with respect to the chain center and exhibiting volume-law entanglement.

system is entangled is determined by the scaling of the regions with short-range singlets. Specifically, our main result is that for $0 < h < \infty$ and finite δ the von Neumann entropy exhibits a square-root scaling behavior as

$$S = C \cdot \ell^{1/2} + k'', \tag{11}$$

where C and k'' are non-universal constants. Notice that equation (11) represents a dramatic violation of the area-law.

2.1. Strong disorder renormalization group (SDRG) method

Away from the limits $h = \delta = 0$, the Hamiltonian (5) can be studied using the SDRG technique, first introduced by Dasgupta and Ma [56]. In the standard SDRG framework, high-energy degrees of freedom in (5) are progressively removed from the model via a decimation procedure. This works as follows. At each SDRG step, we select the link with the largest value of the coupling $J_M \equiv \max\{J_i\}$ (see (3)). Thus, we put in a singlet state the two spins connected by the link. This has the effect of renormalizing the interaction between the next-nearest neighbor spins. This effect can be derived by treating the couplings on the links next to J_M using standard second-order perturbation theory. The resulting effective coupling J' between the next-nearest neighbor spins is obtained as

$$J' = \frac{J_L J_R}{J_M}, \tag{12}$$

where J_L and J_R are the coupling to the left and to the right of J_M, respectively. After many iterations of the SDRG step, all the spins are decimated, and the resulting state is a collection of singlets, i.e. a valence bond state (VBS).

It is useful to rewrite the SDRG procedure by introducing the logarithmic couplings T_m as

$$T_m \equiv -\ln J_m. \tag{13}$$

Notice that T_m takes into account both the random part of the coupling K_m (see (3)), as well as the inhomogeneity due to the presence of h. Notice that the contribution of h is a non-random position-dependent shift in T_m. In the variables T_m the SDRG renormalization step (12) becomes additive. We anticipate that this allows one to interpret the SDRG procedure as a random walk in the space of T_m (see, for instance, section 2.2).

The structure of the SDRG renormalization has been intensively investigated for the homogeneous random [54] XX chain which is obtained for $h = 0$. As it was anticipated, the ground state of the model is described by the random singlet phase. In the RS phase singlets are mostly formed between nearest-neighbor sites, although random singlets connecting spins at arbitrary large distance are also present. Although they are suppressed, the latter are responsible for a slow decay, as a power law, of the spin-spin correlation function. An important observation is that after many SDRG steps the distribution of the renormalized couplings is of the form (4) with $\delta \to \infty$. This implies that the strength of the disorder effectively increases during the SDRG flow, which justifies the use of perturbation approach in (12), and the applicability of the SDRG method. Finally, we should mention that the SDRG approach proved to be the method of choice to understand the entanglement scaling in generic disordered systems [54, 68–80].

Here we choose K_m (see (3)) distributed according to (4). Writing this quantity as $K_m = \xi_m^\delta$, one can easily verify that ξ_m is a random variable uniformly distributed in the interval $[0, 1]$. This allows one to rewrite the couplings T_m as

$$T_m = \begin{cases} h\big(\frac{1}{2} - \frac{\delta}{h}\ln\xi_0\big), & m = 0\,, \\ h\big(|m| - \frac{\delta}{h}\ln\xi_m\big), & |m| > 0\,. \end{cases} \tag{14}$$

An important consequence of (14) is that apart from the overall factor h, the couplings T_m are functions of the ratio δ/h only. Hence, the VBS state obtained at the end of the SDRG, as well as the entanglement entropy, only depends on δ/h.

2.2. Path invariance of the SDRG for the XX chain: a useful lemma

Since in this paper we mostly focus on the random XX chain, here we wish to discuss a crucial simplification that occurs when one applies the SDRG method to this model. We show that for the random XX chain (see (5)) the renormalized coupling between two sites separated by an odd number of consecutive bonds is independent of the decimation pattern, and it has a simple form that we provide. To the best of our knowledge this interesting property has not been noticed before in the literature. In appendix A we propose an algebraic derivation of this property in terms of a triplet product inspired by the SDRG method.

Let us start with the SRDG decimation of the block of four spins shown in figure 3(a), that we denote as $[i - \frac{1}{2}, i + \frac{5}{2}]$, where i is an integer. The renormalization of this block amounts to the formation of a bond between the sites $i + \frac{1}{2}$ and $i + \frac{3}{2}$ and a new effective coupling between the sites $i - \frac{1}{2}$ and $i + \frac{5}{2}$ whose value is given by equation (12),

$$J_{[i-\frac{1}{2},i+\frac{5}{2}]} = \frac{J_i\, J_{i+2}}{J_{i+1}}\,. \tag{15}$$

Working with the logarithmic couplings $T_i = -\ln J_i$, this equation becomes

$$T_{[i-\frac{1}{2},i+\frac{5}{2}]} = T_i - T_{i+1} + T_{i+2}\,. \tag{16}$$

The next example involves the renormalization of the block of six consecutive sites $[i-\frac{1}{2}, i+\frac{9}{2}]$ depicted in figure 3(b). Now there are two possible patterns. In the first one (figure 3(b) top) a nested rainbow diagram with two bonds is formed. The other possibility is to create two bubble diagrams forming the bonds $(i+\frac{1}{2}, i+\frac{3}{2})$ and $(i+\frac{5}{2}, i+\frac{7}{2})$ (figure 3(b) bottom). Using (12), it is straightforward to check that both decimation patterns give the same effective coupling between sites $i-\frac{1}{2}$ and $i+\frac{9}{2}$, which reads

$$T_{[i-\frac{1}{2},i+\frac{9}{2}]} = T_i - T_{i+1} + T_{i+2} - T_{i+3} + T_{i+4}\,. \tag{17}$$

The general expression for the renormalized coupling for a block $[i-\frac{1}{2}, i+n+\frac{1}{2}]$ with $n+1$ bonds is given by

$$T_{[i-\frac{1}{2},i+n+\frac{1}{2}]} = \sum_{j=0}^{n} (-1)^j\, T_{i+j}, \tag{18}$$

where n is the number of spins decimated, that must be an even number. Equations (16) and (17) correspond to the cases $n=2$ and $n=4$ of (18) respectively.

We now prove (18) by general induction. The key step of the proof is summarized in figure 3(c). The boxes in the figure denote renormalized couplings. The numbers n, m, p inside the boxes denote the numbers of spins that have been decimated. To proceed by induction, we assume that equation (18) holds for these renormalized couplings. Now, two spins are left at positions $i+n+\frac{1}{2}$ and $i+n+m+\frac{3}{2}$. Without loss of generality we can assume that these are the two spins that are decimated at the next SDRG step. After the decimation, one obtains that the renormalized coupling connecting sites $i-\frac{1}{2}$ and $i+n+m+p+\frac{5}{2}$ is given as

$$T_{[i-\frac{1}{2},i+n+m+p+\frac{5}{2}]} = T_{[i-\frac{1}{2},i+n+\frac{1}{2}]} - T_{[i+n+\frac{1}{2},i+n+m+\frac{3}{2}]} + T_{[i+n+m+\frac{3}{2},i+n+m+p+\frac{5}{2}]}. \tag{19}$$

Using that all the renormalized couplings appearing in the right hand side in (19) satisfy (18), one obtains that

$$\begin{aligned} T_{[i-\frac{1}{2},i+n+m+p+\frac{5}{2}]} &= \sum_{j=0}^{n} (-1)^j\, T_{i+j} - \sum_{j=0}^{m} (-1)^j\, T_{i+n+1+j} + \sum_{j=0}^{p} (-1)^j\, T_{i+n+m+2+j} \\ &= \sum_{j=0}^{n+m+p+2} (-1)^j\, T_{i+j} \end{aligned} \tag{20}$$

that reproduces equation (18) for the renormalized coupling of the block. This gives the proof of the desired result.

A few comments are in order to show the relevance of our result. First, equation (18) provides an exact mapping between the SDRG flow of the couplings T_i and an *alternating* random walk. This mapping holds true for any distribution of the initial

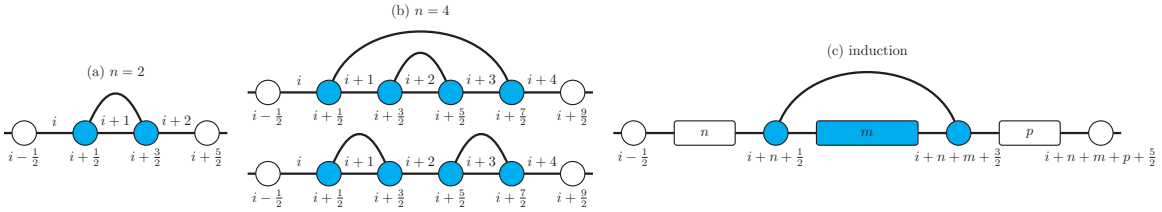

Figure 3. Path invariance theorem for the SDRG in the random XX chain: pictorial proof by induction. The figure shows that the renormalized coupling between two sites $i-\frac{1}{2}$ and $i+n+\frac{1}{2}$ obtained after decimating all the n spins in between does not depend on the decimation pattern. (a) The theorem for $n=2$. Only one decimation pattern is possible. (b) $n=4$. Now two patterns are possible: a rainbow and a bubble pattern (top and bottom, respectively). (c) Induction step to prove the theorem. The boxes denote the renormalized couplings for which the theorem applies.

couplings J_i. However, equation (18) does not contain any spatial information about the SDRG flow. This means that from (18) it is not straightforward to reconstruct the information about the place where the SDRG processes has occurred. This fact represents an obstacle to derive from equation (18) the scaling of correlation functions or of the entanglement entropy. Still, we anticipate that this limitation can be overcome for the random inhomogeneous XX chain in the large h limit (strongly inhomogeneous limit). This happens because the presence of the inhomogeneity provides a simple relation between the SDRG step n and the distance from the chain center. More precisely, sites far away from the chain center are usually renormalized at later stages along the SDRG procedure.

Another important consequence of equation (18) is that, given a region containing n spins, equation (18) allows one to derive the distribution of the renormalized couplings after decimating all the spins. Using the random walk framework, one obtains that this is the distribution of the final position of the walker after n steps. It is straightforward to derive this distribution in the limit $n \to \infty$. Clearly, the sum of the even and odd sequences in equation (18) can be treated separately. Both are the sum of independent identically distributed exponential variables, that follow the gamma distribution. By using that for large n the gamma distribution is well approximated by a normal distribution, one has that the sum of the even and odd terms in equation (18) are distributed with $(\pi n)^{-1/2}\exp[(x-n/2)^2/n]$. The renormalized coupling after n SDRG steps is obtained as the difference between the sum of the odd and even sequences in equation (18). This is again a normal distribution with zero mean and variance n, i.e.

$$P\left(T = T_{[i-\frac{1}{2},i+n+\frac{1}{2}]}\right) = \frac{1}{\sqrt{2\pi n}}\mathrm{e}^{-T^2/(2n)}. \tag{21}$$

2.3. Entanglement entropy of random singlet states

In the following sections we will present numerical results for the von Neumann entropy in the random inhomogeneous XX chain. The results are obtained by using the SDRG method. At the end of the SDRG procedure one obtains a VBS, in which all the spins

are paired forming singlets. For any VBS configuration, the entanglement entropy S between a subsystem A and the rest (see figure 1) is proportional to the number of singlets that are shared between A and its complement $\bar{A}$. It is straightforward to show that for any VBS state, the reduced density matrix ρ_A of subsystem A is written as

$$\rho_A = \bigotimes_{i=1}^{n_{A:A}} \rho_{2S} \bigotimes_{i=1}^{n_{A:\bar{A}}} \rho_S, \tag{22}$$

where $n_{A:A}$ is the number of singlets between spins in A and $n_{A:\bar{A}}$. In (22), ρ_S and ρ_{2S} are the density matrices of a system of one spin and of a singlet, respectively. Specifically, ρ_{2S} is defined as

$$\rho_{2S} = \frac{1}{2}\begin{pmatrix} 0 & 0 & 0 & 0 \\ 0 & 1 & -1 & 0 \\ 0 & -1 & 1 & 0 \\ 0 & 0 & 0 & 0 \end{pmatrix}, \tag{23}$$

in the basis $|\uparrow\uparrow\rangle$, $|\uparrow\downarrow\rangle$, $|\downarrow\uparrow\rangle$, and $|\downarrow\downarrow\rangle$. ρ_{2S} has eigenvalues $0, 1$. The reduced density matrix ρ_S for one of the spins is

$$\rho_S = \frac{1}{2}\begin{pmatrix} 1 & 0 \\ 0 & 1 \end{pmatrix}. \tag{24}$$

Only ρ_S contributes to the von Neumann entropy of subsystem A with the rest. This is because ρ_{2S} has only eigenvalues $0, 1$. This is also physically expected because ρ_{2S} takes into account the singlets between spins in A. The entropy is obtained from (22) to (24)

$$S = n_{A:\bar{A}} \ln 2. \tag{25}$$

From (25) one has that the disorder averaged entropy $\langle S \rangle$ is proportional to the average number of singlets $\langle n_{A:\bar{A}} \rangle$ shared between A and its complement $\bar{A}$.

3. Area-law violation in the random inhomogeneous XX chain

3.1. Von Neumann entropy: SDRG results

We now discuss the scaling behavior of the ground-state von Neumann entropy in the random inhomogeneous XX chain (see (5)). In figure 4 we present numerical data for the von Neumann entropy S of a subsystem A placed at the center of the chain (see figure 1). The results are obtained by implementing the SDRG method discussed in section 2.1. The entropy S is plotted versus the subsystem size ℓ of A. The different symbols in the figure correspond to different values of the inhomogeneity h. The disorder strength parameter δ (see (3)) is fixed to $\delta = 1$. For $h \to \infty$ the model reduces to the rainbow chain, and the volume law $S \propto \ell$ is expected. Oppositely, for $h \to 0$ the homogeneous random XX chain is recovered with logarithmic entanglement scaling (7). Surprisingly, for all the intermediate values of $0.5 < h < 10$, the entropy exhibits a power-law increase with ℓ (notice the logarithmic scale in both axes). A preliminary

analysis suggests the behavior $S \propto \ell^{1/2}$. To perform a more careful finite-size analysis we fit the SDRG results to

$$S = a + b\ell^{1/2}, \tag{26}$$

where a and b are fitting parameters. The results of the fits are reported in figure 4 as dashed-dotted lines. Clearly, for small values of ℓ the data exhibit deviations from (26). This behavior has to be attributed to finite-size corrections, due to the small ℓ. Similar corrections are present for clean models, as well as for the random XX chain [60]. However, already for $\ell \gtrsim 10$ the data are in perfect agreement with (26) for all values of h considered.

Alternatively, in figure 5 we plot the half-chain entropy as a function of the chain length L. The data are now for a wide range of $0 \leqslant \delta \leqslant 64$. The data are for $h = 1$. For $\delta = 0$ the volume law behavior is visible, whereas the data for $\delta = 64$ are suggestive of the logarithmic behavior that is expected in the random singlet phase. For all other values of δ the square root scaling is visible, confirming the results of figure 4.

It is interesting to investigate the combined effect of disorder and inhomogeneity on the scaling of S. This is discussed in figure 6, by considering different values of δ and h. The figure plots S as a function of ℓ for several values of h and δ (different symbols). All the data for different δ and h but with the same value of h/δ collapse on the same curve. This confirms that S is a function of h/δ only, as it was anticipated in section 2.1. The figure shows SDRG results for $h/\delta = 7$ (empty symbols), $h/\delta = 4$ (filled symbols), and $h/\delta = 0.5$ (hatched symbols). This scaling behavior, however, is valid only within the SDRG method. We anticipate that for the random inhomogeneous XX chain the entanglement entropy can be calculated exactly (see section 5) using free-fermion techniques, and it is a function of h/δ only for large h.

Finally, for all values of h, δ considered in figure 6 the von Neumann entropy exhibits the square-root scaling (26). The dashed-dotted lines in the figures are fits to (26), and they are in good agreement with the SDRG results. We should also remark that for $h/\delta = 0.5$ the square root scaling of the von Neumann entropy is visible only for larger $\ell \gtrsim 100$, due to larger finite-size effects, as it is also clear also from figure 4.

3.2. Understanding the area-law violation: bubble versus rainbow regions

The square-root entanglement scaling discussed in figures 4 and 5 can be qualitatively derived from the distribution of the rainbow and bubble regions of the states. To this end we shall define ℓ_r as the number of consecutive concentric bonds that constitute a given rainbow region. For example, in the pure rainbow state we have $\ell_r = L$ bonds connecting the left and right halves of the chain. On the other hand, we define ℓ_b as the number of points that are connected by consecutive dimer bonds that constitute a bubble region (see figure 2). An example of a VBS state for a chain with $2L = 14$ sites is shown in figure 7. This configuration contains two rainbow regions with $\ell_r = 2$ and $\ell_r = 1$ bonds (continuous links), and two bubble regions with $\ell_b = 4$ sites each (see dashed lines in the figure).

To compute the probability distribution of ℓ_r and ℓ_b we apply the SDRG method to decimate all the spins for a set of disorder realizations.

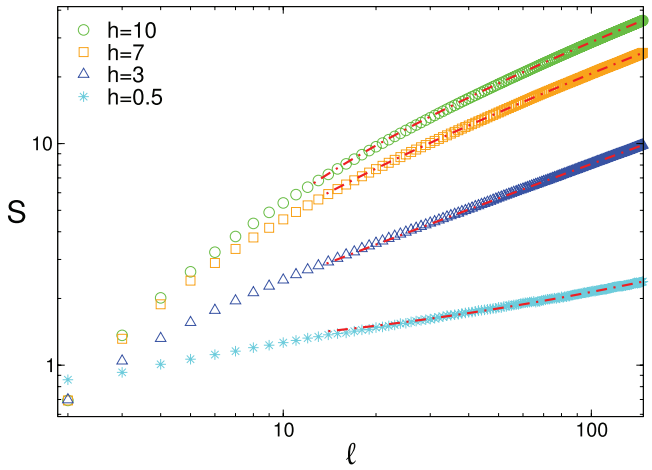

Figure 4. Unusual scaling of the entanglement entropy in the randbow phase: entanglement entropy plotted as a function of the subsystem length ℓ. The subsystem starts from the center of the chain (see figure 1). The data are SDRG results for the random inhomogeneous XX chain. The different symbols are for different values of h and fixed value of $\delta = 1$. Logarithmic scale is used on both axes. The dashed-dotted lines are fits to $a + b\ell^{1/2}$, with a, b fitting parameters.

The distribution of the rainbow bonds $P_r(\ell_r)$ is obtained by constructing the histograms of the values of ℓ_r of the different rainbow regions. An average over different disorder realizations is performed. The resulting histograms for ℓ_r are shown in figure 8. The data are for the random inhomogeneous XX chain in the strongly inhomogeneous limit for $h \gg 1$. We use a logarithmic scale on the y-axis. The data show a clear exponential decay with ℓ_r. The exponential decay is smaller for greater values of h. This is an expected result because in the limit $h \to \infty$ the rainbow regions will start to proliferate.

A similar analysis can be performed for the distribution $P_b(\ell_b)$ of the extension ℓ_b of the bubble regions. The results are reported in figure 9 for $h = 7$ and $h = 10$. Interestingly, on the scale of the figure the two histograms are not distinguishable, signalling that P_b does not depend significantly on h, at least for large h. In stark contrast with the rainbow regions (see figure 8), P_b exhibits a power-law decay with ℓ_b. A careful analysis suggests the behavior

$$P_b(\ell_b) \propto \ell_b^{-3/2}. \tag{27}$$

The dash-dotted line in figure 9 is a fit to the behavior (27), and it perfectly describes the numerical data.

The results of figures 8 and 9 allow one to understand qualitatively the square-root behavior of the von Neumann entropy (11). First of all, since P_r is an exponential function, the average number of rainbow bonds $\langle \ell_r \rangle$ is a constant independent on L,

$$\langle \ell_r \rangle = \int_1^\infty \mathrm{d}x \, x P_r(x) \,, \tag{28}$$

where we have replaced the upper limit of the integral, namely L (total number of bonds) by ∞, without changing essentially the final result. On the other hand, given a

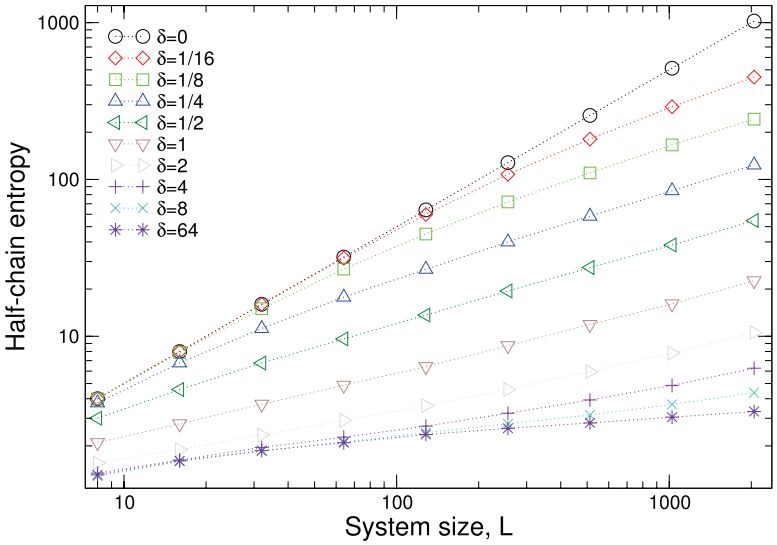

Figure 5. Unusual scaling of the entanglement entropy in the randbow phase: half-chain entanglement entropy plotted as a function of the chain length L. The data are SDRG results for the random inhomogeneous XX chain. The different symbols are for different values of δ and $h = 1$. The data are averaged over 10^4 disorder realizations.

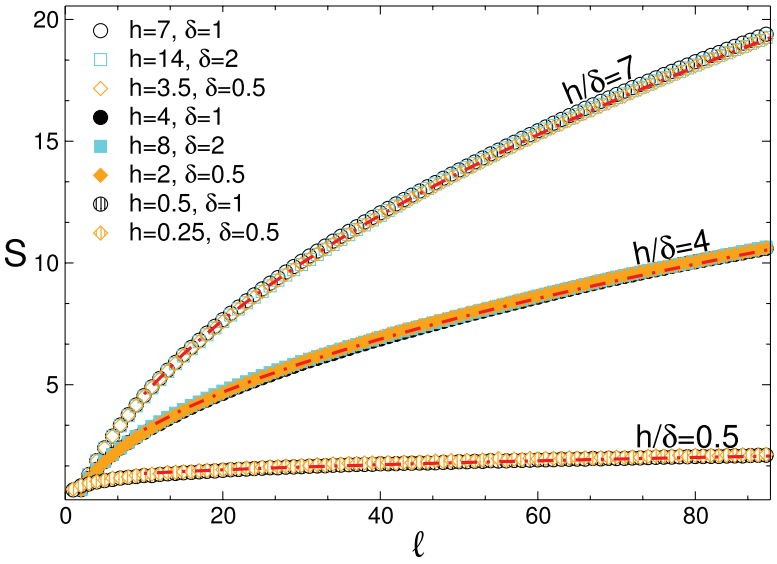

Figure 6. Entanglement entropy S plotted as a function of the subsystem size ℓ: SDRG results for the randbow XX chain. The symbols correspond to several values of δ and h. The data collapse shows that the von Neumann entropy is a function of the ratio h/δ.

subsystem A of length ℓ, the average number of points of the bubble regions contained in A is given by

$$\langle \ell_b \rangle = \int_2^\ell \mathrm{d}x\, x P_b(x) \propto \ell^{1/2}. \tag{29}$$

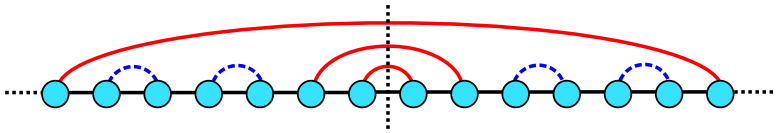

Figure 7. An example of singlet configuration obtained using the SDRG method in the random inhomogeneous XX chain. The limit of strong inhomogeneity $h \gg 1$ is considered. The singlet configuration contains two rainbow regions with two and one long singlets, respectively. These are denoted with continuous lines. A bubble region with four short-range singlet denoted by dashed lines is present.

The short-range singlets forming the bubble phase do not contribute to the entanglement between A and the rest, because they mostly entangle spins within A. The entanglement between A and the rest is due to long range links forming the rainbow phase. However, the scaling of the entropy is determined by the distribution of ℓ_b, which determines the typical spatial separation between the different rainbow regions. A crude estimate of the entanglement entropy is obtained as follows. On average, there are $\langle \ell_r \rangle$ rainbow links every $\langle \ell_b \rangle$ sites. Hence a region A with ℓ sites can be divided roughly into $\ell / \langle \ell_b \rangle$ bubbles separated by $\langle \ell_r \rangle$ rainbow bonds. The von Neumann entropy can then be approximated as

$$S \propto \frac{\ell}{\langle \ell_b \rangle} \times \langle \ell_r \rangle \ln 2 \propto \ell^{1/2} \langle \ell_r \rangle \ln 2, \tag{30}$$

i.e. the square-root scaling in equation (11). Crucially, in (30) we have assumed that the average bubble size $\langle \ell_b \rangle$ and average number of rainbow bonds $\langle \ell_r \rangle$ do not depend on the position in the chain. This might be surprising at first look because the system is not homogeneous. However, as it will be clear in the following sections, due to the form of the renormalization rule (12) and the type of inhomogeneity, the condition that leads to the bubble formation does not depend on the precise SDRG step, and, consequently, on the position in the chain. Notice that this relies on the precise form of (12), which holds only for the XX model, and it breaks down for the interacting XXZ chain.

4. Entanglement contour

It is enlightening to investigate how the square-root scaling of the von Neumann entropy (11) is reflected in the behavior of the entanglement contour. The entanglement contour has been introduced in [81] as a tool to quantify the spatial contributions to the entanglement entropy. The key idea is to write S as the integral of a contour function $s_A(x)$, where $x \in A$. The natural constraints that $s_A(x)$ has to satisfy are

$$S = \int_{x \in A} \mathrm{d}x s_A(x), \qquad s_A(x) \geqslant 0. \tag{31}$$

In (31) we considered a continuous system. The extension to lattice models is obtained by replacing the integrals with the sum over the lattice sites. The first condition in (31) is a normalization, whereas the second ensures that the contribution of each site to the entanglement entropy is positive. Clearly, the conditions (31) are not sufficient to

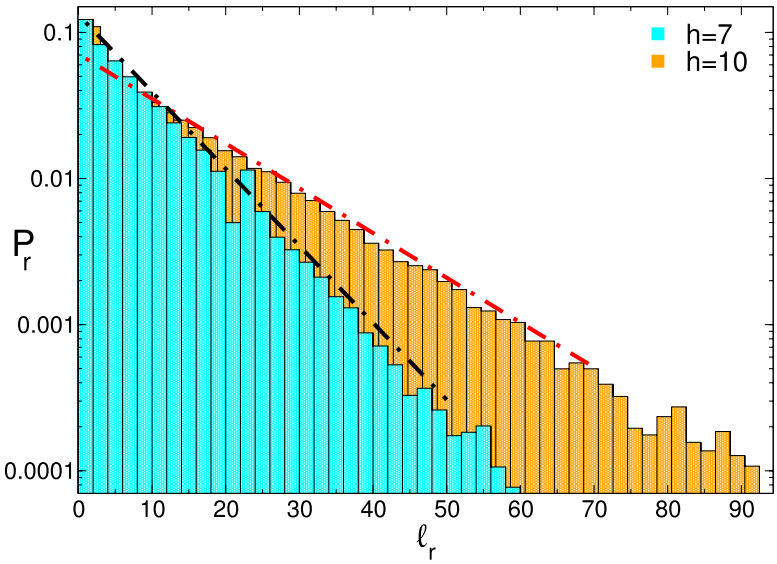

Figure 8. Exponential decaying distribution of the rainbow bonds. The probability $P_r(\ell_r)$ of the number of bonds ℓ_r, of the rainbows. The figure shows normalized histograms for the distribution of ℓ_r. The data are SDRG results for the random inhomogeneous XX chain. The histograms correspond to the values $h = 7, 10$ and $\delta = 1$. Notice the logarithmic scale on the y-axis. The dashed-dotted lines are exponential fits. The data are obtained by averaging over ∼1000 different disorder realizations.

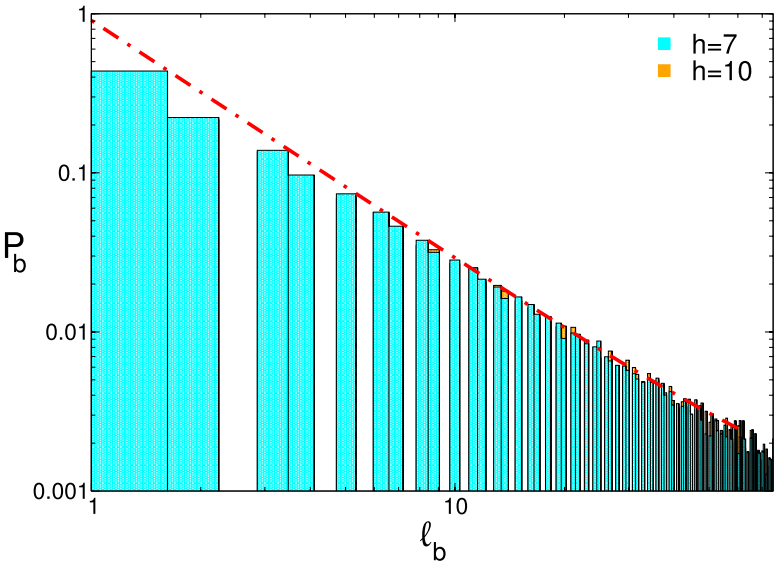

Figure 9. Power law distribution of the size of the bubble regions. The figure shows the probability $P_b(\ell_b)$ of the extension of the bubble regions. Notice the logarithmic scale on both axes. The data are renormalized histograms for the length of the bubble phase in the random inhomogeneous XX chain. The data are are obtained using the SDRG method for a chain with $h = 7, 10$ and $\delta = 1$. Each point is obtained by averaging over ∼1000 disorder realizations. The difference between the histograms for $h = 7$ and $h = 10$ is not visible. The dashed-dotted line is a fit to $\sim x^{-3/2}$.

uniquely identify the contour function s_A. For instance, for an homogeneous system the simplest choice is the flat contour $s_A(x) = S/|A|$, where $|A|$ is the volume of A. However, although this is a legitimate choice, it does not take into account that, due to the area law, most of the contribution to the entanglement between A and its complement $\bar{A}$ originates at the boundary between them. For gapped one and two dimensional systems this boundary locality of the entanglement entropy has been thoroughly investigated in [82] and [83]. We should mention that exact calculations of the contour function s_A are possible only for free models [84, 85], and in conformal field theories [86] (CFT).

Within the SDRG framework for random systems, there is a natural definition of entanglement contour. Precisely, the value of s_A on a given site x of A is $\ln 2$ if there is a link starting at site x and ending in $\bar{A}$, and it is zero otherwise. Numerical results for the contour function $s_A(x)$ in the random inhomogeneous XX chain as a function of the position x in A are shown in figure 10. We have chosen the block A as the right half of the chain that contains L sites.

This figure shows the average contour function $\langle s_A(x)\rangle$ over ∼1000 disorder realizations. The position $x = 1, 2, \ldots, L$ is measured starting from the center of the chain. The figure shows results for several values of $1/64 \leqslant h \leqslant 100$. Clearly, for $h \to \infty$, the ground state of the model is in the rainbow phase (see figure 2(c)). This implies that s_A is flat and $s_A(x) \sim \ln 2$.

In the limit $h \to 0$ the ground state is described by the random singlet phase. This is reflected in the behavior of the contour function s_A. Already for $h = 1/64$ the data in figure (31) exhibit a $\propto 1/x$ decay with x. This implies that for a subsystem of length ℓ one has $S = \int_1^\ell s_A(x)\mathrm{d}x \propto \ln \ell$, which is consistent with the expected result (7). Notice that for $h = 1/64$, for large x, $s_A(x)$ exhibits large oscillations. We do not have an analytic understanding of this behavior, although we should mention that similar oscillations in the entanglement were observed for the clean rainbow XX chain in [86]. Finally, for intermediate values $1/64 < h < 100$ one has $s_A(x) \propto x^{-1/2}$. This is clearly consistent with the square-root scaling behavior $S \propto \ell^{1/2}$, as it was shown in figure 4. Again, this behavior of the contour is a consequence of the power-law scaling of the distribution of ℓ_b. Indeed, the probability that a site at distance $x = \ell$ from the chain center contributes to the entanglement is roughly $1/\langle \ell_b\rangle \sim 1/\ell^{1/2}$.

Finally, we should mention that the knowledge of the contour function allows one to obtain the scaling of the von Neumann entropy for a generic bipartition. For a generic interval with endpoints x_1 and x_2, with $x_2 > x_1$, one obtains

$$S \propto \int_{x_1}^{x_2} \mathrm{d}x x^{-1/2} = x_2^{1/2} - x_1^{1/2}. \tag{32}$$

The validity of (32) is illustrated in figure 11 for the case of a subsystem starting from one of the chain boundaries. In this case equation (32) gives that $S \propto \sqrt{L/2} - \sqrt{L/2 - \ell}$. The figure shows the von Neumann entropy of a subsystem of length ℓ starting from one boundary of the chain, as a function of $2\ell/L$. The data are for a chain with $h/\delta = 1, 2$. The results are SDRG data for a chain with $L = 400$ averaged over ∼1000 disorder realizations. The dashed-dotted lines are fits to

$$S = a + b(\sqrt{L/2} - (L/2 - \ell)^{1/2}), \tag{33}$$

with a, b fitting parameters. The agreement between the numerical data and (33) is perfect, supporting the validity of (32).

5. Numerical benchmarks using the exact solution of the XX chain

In this section we provide exact results for the entanglement entropy of the random inhomogeneous XX chain (5). The key observation is that for any disorder distribution, the XX chain is exactly solvable after mapping it to free fermions. The single-particle eigenstates $|\Psi_q\rangle$ (with q an integer that labels the different eigenstates) of (2) are of the form

$$\eta_q^\dagger|0\rangle \equiv |\Psi_q\rangle = \sum_{i=-L+\frac{1}{2}}^{L-\frac{1}{2}} \Phi_q(i) c_i^\dagger|0\rangle, \tag{34}$$

with $|0\rangle$ denoting the fermionic vacuum, and $\Phi_q(i)$ the eigenstate amplitudes. Here η_q denotes a new fermionic operator creating the single particle excitation. To determine $\Phi_q(i)$ one has to solve the Schödinger equation, which reads

$$-J_{i+\frac{1}{2}}\Phi_q(i+1) - J_{i-\frac{1}{2}}\Phi_q(i-1) = 2\epsilon_q\Phi_q(i), \quad i = \pm\frac{1}{2}, \pm\frac{3}{2}, \ldots, \pm(L-\frac{1}{2}), \tag{35}$$

with $J_L = J_{-L} = 0$, and ϵ_q the single-particle energies. Equation (35) defines the eigenvalue problem for the banded $(2L)\times(2L)$ matrix $T_{i,j} \equiv \frac{1}{2}(J_{j+\frac{1}{2}}\delta_{i,j+1} + J_{j-\frac{1}{2}}\delta_{i,j-1})$. The eigenvalues of T are organized in pairs with opposite sign. This can be shown as follows. Given the amplitude $\Phi_1(i)$ of an eigenvector with $\epsilon_q > 0$, it is straightforward to check that the amplitudes of the eigenvector with eigenvalue $-\epsilon_q$ are obtained as $(-1)^i\Phi_q(i)$. The ground state $|GS\rangle$ of (2) at half filling belongs to the sector with $M = L$ fermions, and it is constructed by filling all the negative modes as

$$|GS\rangle = \eta_{q_M}^\dagger \eta_{q_{M-1}}^\dagger \cdots \eta_{q_1}^\dagger|0\rangle. \tag{36}$$

It is useful for the following to derive the anticommutation relations

$$\{\eta_q^\dagger, c_j^\dagger\} = \{\eta_q, c_j\} = 0, \tag{37}$$

and

$$\{\eta_q^\dagger, c_j\} = \Phi_q(j)\delta_{k,j}, \quad \{\eta_q, c_j^\dagger\} = \Phi^*(j)\delta_{k,j}. \tag{38}$$

Using (37) and (38), the expectation value of the two-point function $\langle c_i^\dagger c_i\rangle$ in a generic eigenstate of (5) reads

$$\langle c_i^\dagger c_j\rangle = \sum_q \Phi_q^*(i)\Phi_q(j), \tag{39}$$

where the sum if over the filled modes q defining the eigenstate.

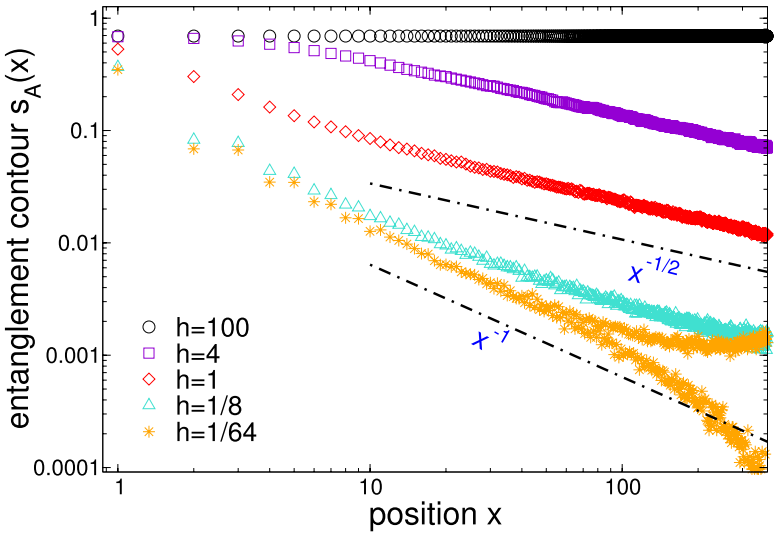

Figure 10. Spatial contributions to the subsystem entanglement entropy S (entanglement contour). The data are SDRG results for the inhomogeneous random XX chain. The figure shows the contour function $s_A(x)$ as a function of the position x inside block A of the chain. The different symbols correspond to different values of h and fixed $\delta = 1$. For $h \to \infty$ the contour is flat and equal to $\ln 2$, implying that all the sites of A contribute equally to the von Neumann entropy, which exhibits volume-law scaling. For intermediate values of $0 < h < \infty$, one has the behavior $x^{-1/2}$, which implies that $S \propto \sqrt{\ell}$. Finally, in the limit $h \to 0$, one has the scaling $s_A \propto x^{-1}$, implying $S \propto \ln \ell$, reflecting the onset of the random singlet phase in that limit.

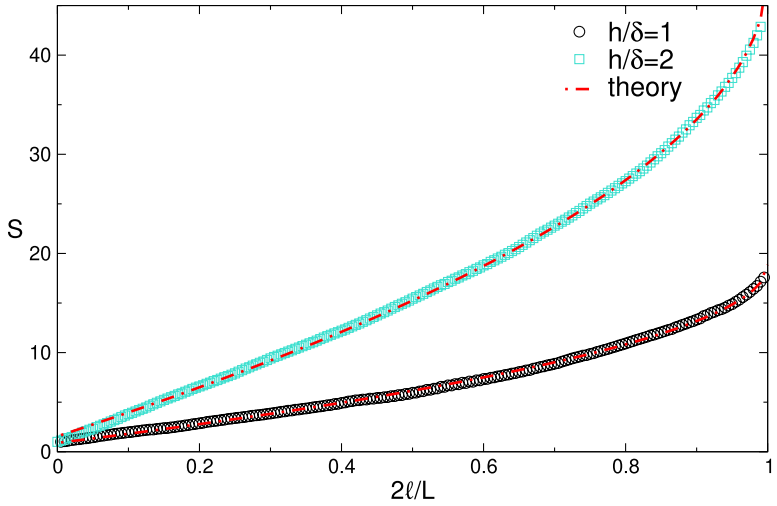

Figure 11. Entanglement entropy of a subsystem starting from one of the boundaries of the chain. The data are SDRG results for the XX chain. The results are for a chain with $L = 400$ sites, and $h/\delta = 1, 2$. The dashed-dotted lines are fits to $a + b(\sqrt{L/2} - (L/2 - \ell)^{1/2})$, with a, b fitting parameters, and ℓ the subsystem length.

Let us now consider the bipartition of the chain in figure 1. For any free-fermion model, even in the presence of disorder, the reduced density matrix ρ_A of subsystem A can be obtained from the correlation matrix [87–92] restricted to A

$$\mathcal{C}_{ij}^{(A)} \equiv \langle c_i^\dagger c_j \rangle, \tag{40}$$

where $i, j \in A$. Moreover, given the eigenvalues λ_k of $\mathcal{C}^{(A)}$, the entanglement entropy S is given as

$$S = -\sum_k (\lambda_k \ln \lambda_k + (1-\lambda_k)\ln(1-\lambda_k)). \tag{41}$$

Numerical results for the von Neumann entropy S obtained using (41) are reported in figure 12 versus the subsystem size ℓ. The figure shows results for a chain with $2L = 100$ sites and several values of h and δ (different symbols in the figure). We should mention that due to the exponential decay of the couplings J_i, the calculation of the eigenvalues λ_j requires to use arbitrary precision routines. The results in figure 12 were obtained requiring precision up to 10^{-80}. To highlight the power-law behavior of S, in the figure we use a logarithmic scale on both axes. Clearly, for all values of h and δ, the data exhibit the behavior $S \propto \ell^{1/2}$. The dashed-dotted lines in the figure are fits to

$$S = a + b\ell^{1/2}, \tag{42}$$

with a, b fitting parameters. For small values of h the asymptotic scaling of S is already visible for $\ell \gtrsim 3$, whereas upon increasing h the asymptotic scaling sets in at larger values of ℓ, as expected. We should also mention that the finite-size effects due to L are negligible. This is expected because the subsystem is placed at the center of the chain. One should observe that all the data shown in the figure correspond to the same value of $h/\delta = 3$. Surprisingly, no data collapse is observed, suggesting that the entropy is not a function of the ratio h/δ only. This is in contrast with the SDRG data (see figure 6), for which the scaling with h/δ holds.

6. Energy gap

It is interesting to investigate the relation between the square-root scaling of the von Neumann entropy and the scaling of the energy gap of the model. For the Fredkin and Motzkin spin chains this has been investigated in [93–95]. This analysis is presented in figure 13. In the figure we discuss the scaling behavior of the energy gap in both the random XX chain (see section 5) and within the SDRG formalism. For the XX chain the gap is calculated exactly as the difference $\Delta E = E_1 - E_0$, with E_0 and E_1 the ground state and the first excited state of the chain. In the SDRG formalism, a good estimate for the energy gap is the final value of the renormalized coupling, which will often correspond to a long distance bond from site $-L$ to site $+L$. In this case, we may use equation (18) to estimate the energy gap:

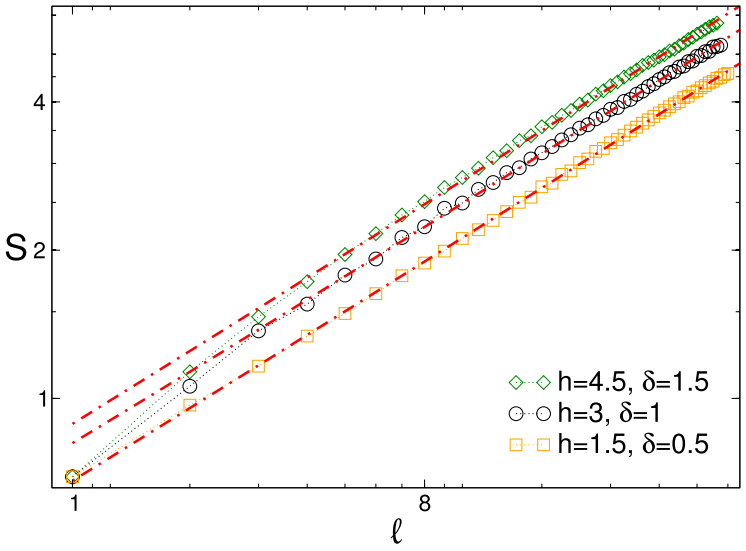

Figure 12. Entanglement entropy S in the random inhomogeneous XX chain: exact results. The figure shows S obtained using free-fermion techniques plotted versus the size ℓ of the subsystem. Note the logarithmic scale on both axes. The symbols are the data for a chain with $2L = 100$ sites and several values of h and δ. Each point is obtained by averaging S over 500 different disorder realizations. The dashed-dotted line is a fit to the expected behavior $S = a + b\ell^{1/2}$, with a, b fitting parameters. Notice that S is not a function of the ratio h/δ only.

$$-\ln(\Delta E_{\rm SDRG}) = h\left[\frac{(-1)^L}{2} + 2\sum_{j=0}^{L-1}(-1)^j(L-j)\right] - \delta\sum_{j=0}^{2L}(-1)^j \log \xi_{j-L}. \quad (43)$$

It is straightforward to show that the disorder-average of the gap and the standard deviation of the fluctuations are given as

$$\langle -\ln(\Delta E_{\rm SDRG})\rangle \propto h(L+1/2) \quad (44)$$

$$\sigma(-\ln(\Delta E_{\rm SDRG})) \propto \delta\sqrt{2}L^{1/2}. \quad (45)$$

Here we neglect additive constant terms. The correctness of (44) and (45) is discussed in figure 13. Panels (a) and (b) focus on the mean value of the energy gaps and its fluctuations, respectively. The figure shows both exact results for the XX chain (circles) as well as numerical SDRG data (diamonds). For the XX chain the data are for a chain up to $L = 100$, whereas for the SDRG data we show results up to $L = 500$. In both cases we average over ∼1000 disorder realizations. The figure show $\langle -\ln \Delta E\rangle$ and the standard deviation of its fluctuations $\sigma(-\ln \Delta E)$ plotted as a function of L. In (a) and (b) the dashed-dotted lines are the theoretical results equations (44) and (45), respectively. First, it is remarkable that the SDRG results are in *quantitative* agreement with the data for the XX chain. Moreover, in both panels the theory predictions (44) and (45) are in perfect agreement with the numerical data.

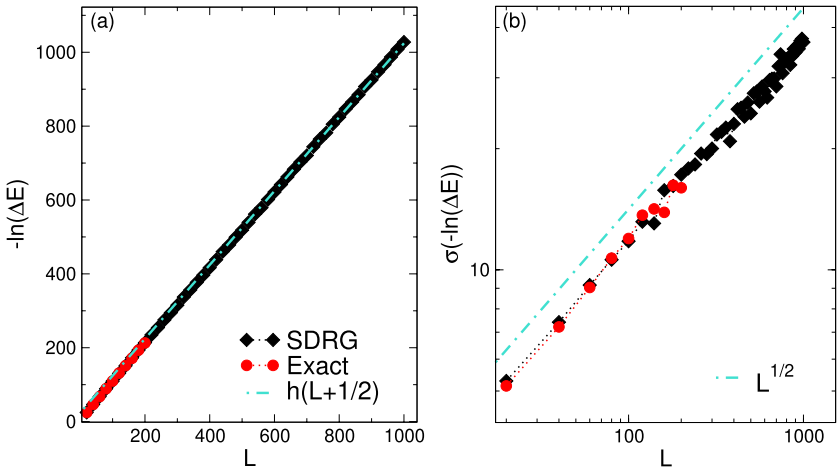

Figure 13. Energy gap of the random inhomgeneous XX chain. Panels (a) and (b) show the mean energy gap $\langle -\ln \Delta E \rangle$ and the standard deviation $\sigma(-\ln \Delta E)$ of its fluctuations, respectively. The x-axis shows the chain length L. In both figures, circles are exact results for the XX chain up to $L = 100$, whereas the diamonds are SDRG data up to $L = 500$. The disorder average is over 1000 disorder realizations, and we use $h = \delta = 2$. The dashed-dotted lines are the theoretical SDRG results.

7. A toy model for the strongly inhomogeneous limit

In this section we discuss the strongly inhomogeneous limit of the random XX chain (see (5)), which is obtained for $h \to \infty$ in (3). In this limit, several analytical results can be obtained, for instance the scaling of the survival probabilities for the rainbow and the bubble regions presented in figures 8 and 9. For $h \gg 1$, the ground state of (5) has the structure presented in figure 2(b). This consists of long links forming a 'rainbow' phase connecting distant spins across the chain center, and of short links connecting spins on neighboring sites, forming a 'bubble' phase. Importantly, for large h all the link configurations are symmetric with respect to the center of the chain. This is due to the fact that for large h, more degrees of freedom (bonds), which are decimated first, which are nearer to the center of the chain. This implies that SDRG decimations happen symmetrically with respect to the chain center. To further enforce this symmetry in the following we will restrict ourselves to symmetric couplings, i.e. $K_n = K_{-n}$ (see (3)). A crucial consequence of the large h limit is that the net effect of the SDRG procedure, at any step, is to renormalize the central coupling J_0 (see (2)). Moreover, the VBS state obtained at the end of the renormalization is constructed using only two types of diagrams that we term 'rainbow diagrams' and 'bubble diagrams'. A typical singlet configuration is depicted in figure 14(a). The building blocks, i.e. rainbow and bubble diagrams, are better discussed in figures 14(b) and (c), respectively. In both (b) and (c) the coupling $J_0^{(n+1)}$, connecting sites $n+1$ and $-n-1$, is the renormalized coupling obtained after decimating the first $2n$ spins around the chain center (in this section the position of the spins are labelled by integers: $\pm 1, \pm 2, \ldots, \pm L$). In the following we derive exact analytic expressions for $J_0^{(n+1)}$. Also, by using (18) we establish a relation between the survival probability of the rainbow and bubble diagrams with certain survival probabilities of an alternating random walk.

7.1. Rainbow diagrams: random walk and survival probability

Here we discuss the renormalized coupling obtained from the rainbow configuration illustrated in figure 14(b). First, the initial coupling $J_0^{(n+1)}$ can result from both rainbow and bubble configurations. We now consider the effect of a rainbow diagram of k links. This is obtained by decimating $k+1$ spin pairs around the chain center. Using the strong disorder RG rule (12) the renormalized coupling $J_0^{(n+k+1)}$ that connects the spins at sites $n+k+1$ and $-n-k-1$ is given as

$$J_0^{(n+k+1)} = [J_0^{(n+1)}]^{(-1)^k} \Big[\prod_{\alpha=0}^{k-1} \Big(J_{n+\alpha+1} J_{-(n+\alpha+1)} \Big)^{(-1)^\alpha} \Big]^{(-1)^{k-1}} . \tag{46}$$

As in equation (18), it is useful to take the logarithm of (46) obtaining

$$-\ln J_0^{(n+k+1)} = (-1)^{k-1} \Big[-X_0^{(n+1)} + \sum_{\alpha=0}^{k-1} (-1)^\alpha (X_{n+\alpha+1} + X_{-n-\alpha-1}) \Big] + (n+k+1/2)h. \tag{47}$$

Here we defined $X_j \equiv -\ln K_j$. In (47), the term $(n+k+1/2)h$ is the contribution of the inhomogeneity (see (3)). Importantly, in (47), $X_0^{(n+1)}$ is obtained from $-\ln J_0^{(n+1)}$ by considering only the contributions of K_j (see (3)), i.e. it does not take into account the contribution of h, which is included in the last term in (47). Crucially, here we are using that the h-dependent term in (47) does not depend on the renormalization pattern leading to $J_0^{(n+1)}$. This is a simple consequence of (18). Specifically, we observe that the h-dependent term in $-\ln J_0^{(n)}$ is $(n-1/2)h$, from which the last term in (47) follows. This is easy to prove by induction. The proof is a simpler version of that for (18). One first assumes that after decimating all the spins between sites n and $-n$ the h-dependent contribution to the coupling is given by $(n+1/2)h$. Then one considers the two possible SDRG processes, which consist in adding a rainbow link between the spins at $(n+1)$ and $-(n+1)$, or two short links connecting spins $(n+1)$ and $(n+2)$ and the spins $-(n+1)$ and $-(n+2)$, respectively. It is trivial to verify that in both cases the formula holds.

It is important to observe in (47) the overall alternating term $(-1)^{k-1}$ and the alternating term $(-1)^\alpha$. We anticipate that the former is crucial to determine the survival probability of the rainbow diagrams. Here we are interested in the probability that the rainbow diagram survives k successive SDRG decimation steps. Crucially, while this survival probability could depend on the history of SDRG process, for the XX chain this is not the case, as we are going to show. Given a rainbow diagram of length k, we start by calculating the probability for the diagram to survive for an extra SDRG step. In terms of the couplings J_i (see (3)), the survival condition is

$$J_0^{(n+k+1)} > J_{n+k+1}, \tag{48}$$

which ensures that an extra rainbow link is created by decimating the spins at positions $-n-k-1$ and $n+k+1$. Equivalently, in terms of the logarithmic variables X_k (see (47)) equation (48) reads

$$(-1)^{k-1} \Big[X + \sum_{\alpha=0}^{k-1} (-1)^\alpha X_{n+\alpha+1} \Big] < \frac{h}{4} + \frac{1}{2} X_{n+k+1}, \tag{49}$$

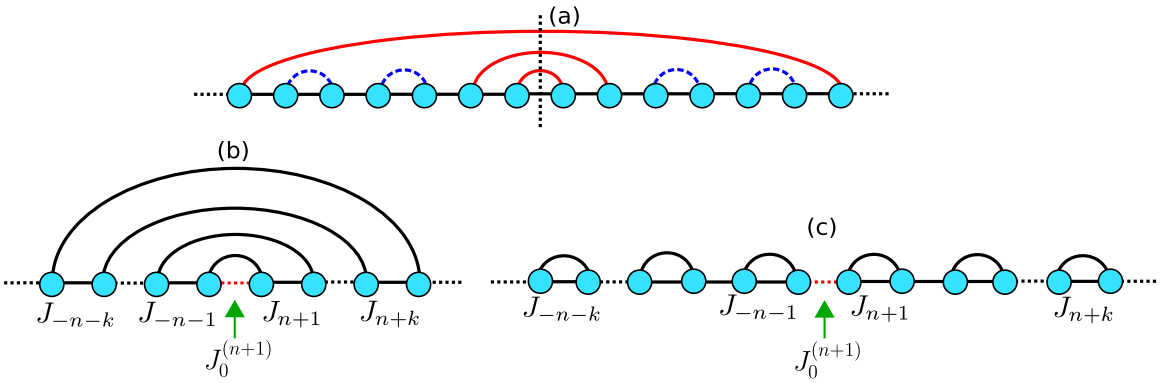

Figure 14. (a) Typical singlet configuration in the ground state of the random inhomogeneous chain in the limit $h \gg 1$. The continuous lines denote long-range singlets ('rainbow' configurations), whereas the dashed ones are short-range singlets connecting spins on nearest-neighbor sites and forming the 'bubble' phase. Notice that only symmetric link configurations with respect to the center of the chain (marked by the vertical line) are allowed. (b) A rainbow diagram formed by long links connecting distant spins across the chain center. The renormalized central link $J_0^{(n+1)}$ results from link configurations as in (a). The length of the diagram is denoted as k. (c) Bubble diagram of length k formed by short singlets joining spins on nearest-neighbor sites. Notice in both (b) and (c) the symmetry with respect to the chain center. In the limit $h \to \infty$ typical bond configurations as in (a) are obtained by combining rainbow and bubble diagrams ((b) and (c)).

where we used that $X_\alpha = X_{-\alpha}$ and we defined $X = -X_0^{(n+1)}/2$ as the starting point of the random walk. The survival probability condition (49) does not depend on n and k. The linear term in $n + k$ in (47) cancels out with the h dependent term in J_{n+k+1}. We anticipate that this is not the case in presence of interactions, i.e. for the XXZ chain, and it will have striking consequences for the scaling of the von Neumann entropy (see section 8). To further simplify the condition (49), in the following we shall neglect the term X_{n+k+1}. For large enough h this should be allowed because X_{n+k+1} is exponentially distributed in $[0, \infty]$. The condition in equation (49) has a simple interpretation in terms of random walks. Due to the factor $(-1)^{k-1}$ the rainbow survival probability is the probability of a walker to stay below $h/4$ if $(k-1)$ is even and above $-h/4$ if $(k-1)$ is odd, remaining confined in the alternating strip $[-h/4, h/4]$. This is illustrated pictorially in figure 15(a). Interestingly, the probability that the walker survives within the strip for n steps decays *exponentially* with n. The details of the calculation are reported in appendix B.

7.2. Bubble diagrams: random walk and survival probability

We now discuss the survival probability for the bubble diagram. The typical bubble diagram is shown in figure 14(c), and it consists of a sequence of short-range singlets between nearest neighbor spins. Here we restrict ourselves to the situation in which the bubble diagrams appear in pairs (i.e. symmetrically) around the chain center, which is a consequence of the choice $J_m = J_{-m}$. Similar to the rainbow diagrams, the net effect of bubble diagrams is to renormalize the central coupling $J_0^{(n+1)}$. After a repeated

application of the SDRG rule (12), the renormalized coupling $J_0^{(n+1+2k)}$ for the diagram in figure 14(c) is given as

$$J_0^{(n+1+2k)} = J_0^{(n+1)} \prod_{\alpha=0}^{2k-1} \left[J_{n+\alpha+1} J_{-n-\alpha-1} \right]^{(-1)^{\alpha+1}}. \tag{50}$$

It is convenient to use logarithmic variables to obtain

$$-\ln J_0^{(n+1+2k)} = X_0^{(n+1)} + \sum_{\alpha=0}^{2k-1} (-1)^{\alpha-1} (X_{n+\alpha+1} + X_{-n-\alpha-1}) + (n+2k+1/2)h. \tag{51}$$

Again, the flow of the renormalized coupling in (51) can be interpreted as a random walk with starting point $X_0^{(n+1)}$. In contrast to the rainbow, there is no overall oscillating term $(-1)^{k-1}$, and the walker can only make an even number of steps, because bubbles are produced in pairs. The last term in (51) encodes the inhomogeneity contribution to the renormalized coupling, and it is independent on the renormalization pattern, as for the rainbow diagram. The condition for the bubble diagram to survive two SDRG steps is

$$J_0^{(n+1+2k)} < J_{n+1+2k}. \tag{52}$$

In the logarithmic variables one finds

$$X + \sum_{\alpha=0}^{2k-1} (-1)^{\alpha-1} X_{n+\alpha+1} > \frac{h}{4} + \frac{1}{2} X_{n+2k+1} \tag{53}$$

where now the starting point of the random walk is defined as $X = X_0^{(n+1)}/2$. Similar to the rainbow, in the following we neglect the term X_{n+2k+1} in (53), because it does not affect the qualitative behavior of the results. In the random walk language, the condition (53) defines the probability that the walker stays above the line $h/4$, as depicted in figure 15(b). Importantly, the survival condition does not depend on the SDRG step, due to the cancellation of the linear term in n in (52). Now, the probability that the walker satisfies (53) for n steps decays as $n^{-3/2}$, in contrast with the rainbow survival probability, which decays exponentially. This is a standard calculation in the random walk literature. We report the details in appendix B.

8. Entanglement entropy in the interacting case

Having established that in the random inhomogeneous XX chain the entanglement entropy exhibits an unusual area-law violation, it is natural to investigate whether this scenario survives in the presence of interactions. In this section we show that the square-root scaling of the entropy (11) is very fragile, and it does not survive if the model is interacting. To be specific, here we consider the inhomogeneous random Heisenberg XXZ chain. This is defined by the Hamiltonian

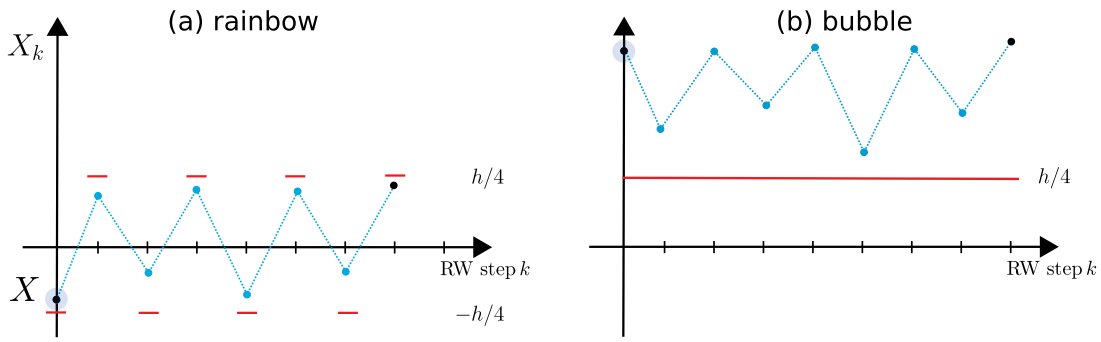

Figure 15. Random walk interpretation of the rainbow and bubble diagrams (see figures 14(b) and (c), respectively). (a) The probability for a rainbow diagram to survive k SDRG steps is mapped to the probability for an *alternating* random walk to be confined in the alternating strip between $[-h/4, h/4]$ for k consecutive steps. (b) The probability for a bubble phase to survive k SDRG steps is the probability for the random walk to stay above the line $h/4$ for k consecutive steps. In both (a) and (b) the initial point of the walker x is related to the renormalized central bond J_0 in figures 14(b) and (c).

$$H = \sum_{i=1}^{L-1} J_i \Big\{ \frac{1}{2} \Big[S_i^+ S_{i+1}^- + S_i^- S_{i+1}^+ \Big] + \Delta S_i^z S_{i+1}^z \Big\}. \tag{54}$$

Here Δ is an anisotropy parameter. The XXX chain corresponds to the isotropic limit $\Delta = 1$. In (54), J_i are the same as in (3). For simplicity, we choose $J_i = J_{-i}$. The SDRG method for the Heisenberg chain is similar to that for the XX chain. The only difference (see (12)) is a factor $1 + \Delta$ in the coupling renormalization [54]. Precisely, the SDRG rule for the renormalized coupling J' in the XXZ chain now reads [70]

$$J' = \frac{J_L J_R}{(1 + \Delta) J_M}, \tag{55}$$

where, as in (12), J_M is the largest coupling. In the random *homogeneous* XXZ chain (i.e. for $h = 0$) the factor $1 + \Delta$ in (55) is irrelevant in the scaling limit of large systems. For instance, the SDRG fixed point describing the ground state is the same for both the XX and the XXX chain. This implies that universal properties are the same for both models. The entanglement entropy exhibits the logarithmic growth (7), and the prefactor of the logarithm does not depend on Δ.

The goal of this section is to show that in the presence of inhomogeneous couplings the factor $1 + \Delta$ in (55) dramatically changes this picture, at least within the framework of the SDRG method. The results are discussed in figure 16. The figure shows SDRG data for the von Neumann entropy S of a subsystem at the center of the chain plotted as a function of the subsystem size ℓ. The continuous lines in the figure correspond to several values of the inhomogeneity parameter h and $\Delta = 1$. Surprisingly, for all values of h, S saturates in the limit $\ell \to \infty$. For $h = 8$ there is a large intermediate region where the square-root scaling behavior (11) holds. This signals the presence of an h dependent crossover length scale ξ_h separating the square-root behavior from the saturating behavior at $\ell \to \infty$. This behavior changes dramatically for $\Delta < 0$. For instance, the dashed line in figure 16 denotes the SDRG data for $h = 2$ and $\Delta = -1/2$.

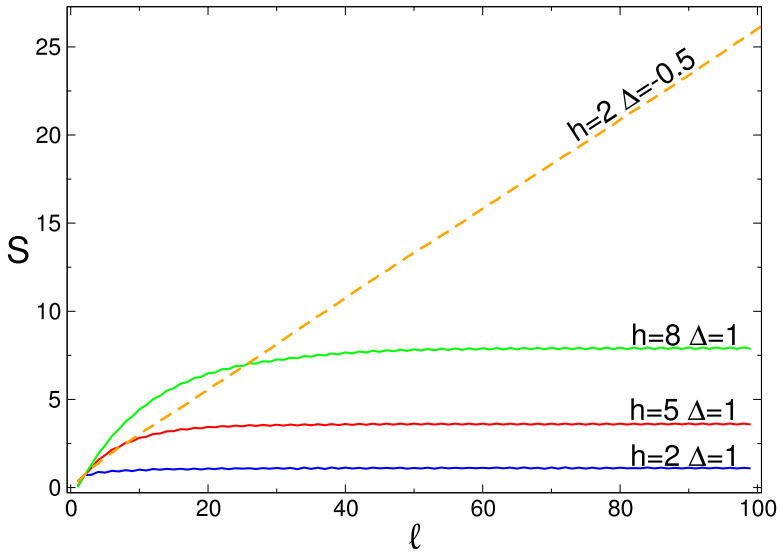

Figure 16. Scaling of the entanglement entropy in an interacting inhomogeneous model. The figure shows the von Neumann entropy S as a function of ℓ, ℓ being the subsystem size. The curves are SDRG results for the randbow XXZ chain for different values of h and Δ. In contrast with the XX chain, S exhibits a saturating behavior for $\Delta > 0$, whereas the volume-law behavior $S \propto \ell$ is observed for $\Delta < 0$. In particular, the dashed-dotted line is the SDRG result for $\Delta = -0.5$ and $h = 2$.

Clearly, the entanglement entropy exhibits the volume-law scaling $S \propto \ell$. We numerically observed that this volume-law scaling happens generically for $\Delta < 0$.

8.1. Random walk interpretation

We now discuss the origin of the behavior observed in figure 16. Here we focus on the limit $h \gg 1$, where one can exploit the mapping between the SDRG flow and the alternating random walk. First, in the large h limit, similar to the non-interacting case, higher-energy degrees of freedom are nearer to the chain center, and are decimated first. This implies that the effect of the SDRG procedure is to renormalize the central coupling, similar to the XX chain. It is also natural to expect that for large h the most likely SDRG patterns are the rainbow and bubble patterns discussed in figures 14(b) and (c).

To proceed, we first discuss the renormalization of J_0 due to a rainbow diagram of length k (see figure 14(b)). A straightforward calculation gives

$$J_0^{(n+k+1)} = (1+\Delta)^{-k \bmod 2} (J_0^{(n+1)})^{(-1)^k} \Big[\prod_{\alpha=0}^{k-1} \Big(J_{n+\alpha+1} J_{-(n+\alpha+1)} \Big)^{(-1)^\alpha} \Big]^{(-1)^{k-1}}. \tag{56}$$

Notice that the renormalized coupling $J_0^{(n+k+1)}$ depends on the parity of k. The condition for the rainbow diagram to survive one SDRG step is still given by equation (48), and in the logarithmic variables X_i we have

$$(-1)^{k-1} \Big[X + \sum_{\alpha=0}^{k-1} (-1)^{\alpha-1} X_{n+\alpha+1} \Big] \lesssim \frac{h}{4} - \frac{\ln(1+\Delta)}{2} (k \bmod 2). \tag{57}$$

The condition (57) is the same as for the XX chain apart from the parity dependent term $\ln(1+\Delta)/2$. However, this extra term is not expected to change the qualitative behavior of the survival probability. Specifically, in the framework of the random walk (compare with figure 15(a)), one has that the walker is now constrained to stay below $h/4 - \log(1+\Delta)/2$ if k is odd, and above $-h/4$ if k is even, i.e. in a strip that is not symmetric around zero (compare with figure 15). It is natural to expect that the decay of the survival probability for the walker will remain exponential.

In stark contrast, the factor $1+\Delta$ in (55) has striking consequences for the survival probability of the bubble diagrams (see figure 14(c)). The renormalized coupling J_0 due to a bubble diagram of length $2k$ reads

$$J_0^{(n+1+2k)} = (1+\Delta)^{-2k} J_0^{(n+1)} \prod_{\alpha=0}^{2k-1} \left[J_{n+\alpha+1} J_{-n-\alpha-1} \right]^{(-1)^{\alpha+1}}. \tag{58}$$

Using equation (58), the condition equation (52) for the survival of the bubble phase can be rewritten as

$$X + \sum_{\alpha=0}^{2k-1} (-1)^{\alpha-1} X_{n+\alpha+1} \gtrsim \frac{h}{4} - k \ln(1+\Delta). \tag{59}$$

In contrast with the non-interacting case, the condition (59) depends on the step k of the walker. This means that for $\Delta > 0$ the survival condition (59) for the walker to be above the line $h/4 - k\ln(1+\Delta)$ is always satisfied for large k. Physically, this suggests that the bubble phase becomes more and more stable as its size increases. However, the short-range singlets in the bubble phase do not contribute to the entanglement entropy, which explains the saturating behavior observed in figure 16. On the other hand, for $\Delta < 0$ one has that for large k the condition (59) is never verified. This implies that the bubble phase is suppressed and the ground state of the model is in the rainbow phase, with volume-law entanglement.

9. Conclusions

In this paper, we have provided evidence of an unusual violation of the area law in a random inhomogeneous one-dimensional model. Specifically, we showed that in a random inhomogeneous XX chain the ground-state entanglement entropy grows with the square root of the subsystem length. We derived this result by mapping the SDRG renormalization flow to an alternating random walk. The exponent 1/2 of the entanglement growth can be understood from certain survival probabilities of the random walk. We also investigated the effect of interactions, considering the random inhomogeneous XXZ chain. The unusual area-law violation is very fragile, and it does not survive when interactions are present.

It is worth mentioning some research directions for future investigation. First, it would be interesting to further study the structure of the renormalization group flow in the light of the result (18). For instance, it is natural to wonder whether (18) might be the starting point for an alternative derivation of the Refael and Moore result [58] for

the entanglement entropy in the random XX chain (as well as for the Rényi entropies in [61]). Another question concerns the fate of the unusual area-law violation in the limit of weak inhomogeneity. In the clean case, i.e. without disorder, using the approach of [96] it has been shown that the model can be mapped to a CFT in curved space-time [67, 86], but what happens to this scenario in the presence of randomness is still unknown. Also, it would be important to extend the analysis performed in this work to other entanglement-related quantities, such as the Rényi entropies, the entanglement spectrum and Hamiltonian, and the logarithmic negativity.

Going beyond the behavior of the XX spin-chain, it would be very useful to thoroughly investigate the phase diagram of the random inhomogeneous XXZ chain. For instance, while for strong inhomogeneity we observed that the entanglement entropy has a volume-law scaling for $\Delta < 0$, the regime of weak inhomogeneity remains unexplored. The most relevant question would be to understand whether the volume-law behavior holds true at any value of the inhomogeneity or if there is a transition to the expected behavior (7) taking place at finite inhomogeneity. Another natural question is whether the mapping between the SDRG flow and the random walk allows one to obtain different exotic area-law violations, such as a power-law growth of the entanglement with an exponent $\alpha \neq 1/2$. A possibility would be to explore the effects of spatially-correlated disorder, that in the homogenous case are known to dramatically affect the critical behavior [54, 55]. Moreover, the nature of the transition between the volume-law and the area-law entanglement in the random inhomogeneous XXZ chain has still to be clarified.

Finally, an independent, but very timely research direction would be to understand how the anomalous scaling of the ground-state entanglement can affect the out-of-equilibrium behavior of the random inhomogeneous XX chain after a (local or global) quantum quench, in particular for the entanglement evolution [97, 98]. For instance, for another model with similar anomalous behavior, the spreading of quantum correlations, turned out to be very peculiar [45].

Acknowledgments

SNS has been supported by the Spanish grant No. FIS2015-66020-C2-1-P. JRL and GS have been supported by the Spanish grants No. FIS2015-69167-C2-1-P, QUITEMAD+S2013/ICE-2801 and SEV-2016-0597 of the 'Centro de Excelencia Severo Ochoa' Programme. VA acknowledges support from the European Union's Horizon 2020 under the Marie Sklodowoska-Curie grant agreement No 702612 OEMBS. PC acknowledges support from ERC under Consolidator grant number 771536 (NEMO). Part of this work has been carried out during the workshop 'Quantum paths' at the Erwin Schrödinger International Institute for Mathematics and Physics (ESI) in Vienna, and during the workshop 'Entanglement in Quantum Systems' at the Galileo Galilei Institute (GGI) in Florence.

Appendix A. SDRG and ternary algebras

In this appendix we propose an algebraic interpretation of the SDRG procedure that gives a simple explanation of the associativity lemma described in section 2.2. We start

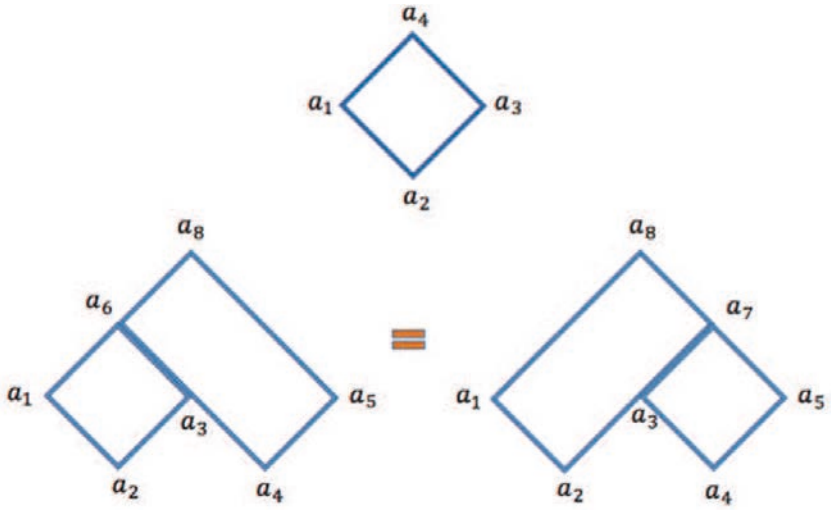

Figure A1. Top: geometric representation of the ternary product $a_4 = \{a_1, a_2, a_3\}$ (see equation (A.1)). Fixing the position of the vertices a_1, a_2 and a_3, of the parallelogram determines the position of the fourth one, a_4. Bottom: depiction of the products: $\{\{a_1, a_2, a_3\}, a_4, a_5\} = \{a_6, a_4, a_5\} = a_8$ and $\{a_1, a_2, \{a_3, a_4, a_5\}\} = \{a_1, a_2, a_7\} = a_8$, that is represented by the corner shaped region with the top vertex a_8 (see A.3)).

by defining an algebra $\mathcal{A}$ with a ternary product, that is, a map between three ordered elements into a fourth one,

$$\begin{aligned} &\mathcal{A} \times \mathcal{A} \times \mathcal{A} \to \mathcal{A} \\ &(a_1, a_2, a_3) \to a_4 = \{a_1, a_2, a_3\}\,. \end{aligned} \tag{A.1}$$

Algebras with a binary product, say $a_1 \cdot a_2$, are called associative if the following condition holds: $(a_1 \cdot a_2) \cdot a_3 = a_1 \cdot (a_2 \cdot a_3)$. Similarly, a ternary algebra is called associative if the triplet product of five elements satisfy [99]

$$\{\{a_1, a_2, a_3\}, a_4, a_5\} = \{a_1, \{a_2, a_3, a_4\}, a_5\} = \{a_1, a_2, \{a_3, a_4, a_5\}\}\,, \tag{A.2}$$

and it is called partially associative if the less restrictive condition holds

$$\{\{a_1, a_2, a_3\}, a_4, a_5\} = \{a_1, a_2, \{a_3, a_4, a_5\}\}\,. \tag{A.3}$$

An associative algebra is obviously partially associative but not vice versa necessarily. Graphical representations of the ternary product (A.1) and the partial associativity condition (A.3) are given in figure A1. An example of ternary algebra is given by the set on non zero complex numbers, $\mathcal{A} = \mathbb{C} - \{0\}$ with product

$$\{a_1, a_2, a_3\} = \alpha \frac{a_1 a_3}{a_2}, \qquad \alpha \neq 0\,. \tag{A.4}$$

This definition yields

$$\begin{aligned} \{a_1, \{a_2, a_3, a_4\}, a_5\} &= \frac{a_1 a_3 a_5}{a_2 a_4}, \\ \{\{a_1, a_2, a_3\}, a_4, a_5\} = \{a_1, a_2, \{a_3, a_4, a_5\}\} &= \alpha^2 \frac{a_1 a_3 a_5}{a_2 a_4}, \end{aligned} \tag{A.5}$$

which shows that $\mathcal{A}$ is partially associative for any $\alpha \neq 0$, and associative only for $\alpha = \pm 1$. Notice that the product (A.4) coincides with the SDRG equation (55) of the XXZ model, under the identification $\alpha = 1/(1+\Delta)$. Hence the algebra corresponding to the XX model is associative, a result that provides an algebraic derivation of the path invariance of the renormalized coupling described in section 2.2. Indeed, the cartoon at the top of figure 3(b) can be seen to correspond to the products

$$\{J_i, \{J_{i+1}, J_{i+2}, J_{i+3}\}, J_{i+4}\}\,, \tag{A.6}$$

while the cartoon at the bottom of figure 3(b) correspond to the products

$$\{\{J_i, J_{i+1}, J_{i+2}\}, J_{i+3}, J_{i+4}\} = \{J_i, J_{i+1}, \{J_{i+2}, J_{i+3}, J_{i+4}\}\}\,. \tag{A.7}$$

The equality between (A.6) and (A.7) amounts to the associativity of the ternary product. Finally, the case $\alpha = -1$, can be shown to correspond to the SDRG of a free fermion which is equivalent to that of the XX model.

Appendix B. Survival probabilities: exact results

We now proceed to calculate the survival probability for the alternating random walks shown in figures B1(a) and (b) (see also figure 15). In the following we will employ standard techniques for the random walk (see, for instance, [100] and [101]). The main result of this section will be an exact formula for the survival probabilities for the alternating walks in figures B1(a) and (b).

B.1. Rainbow diagram

We start discussing the alternating random walk in figure B1(a). Due to the alternating structure of the random walk, it is first convenient to calculate the probability that the walker survives an even number of steps. The building blocks are the probabilities $P_r^{(\vee)}(x, x'')$ and $P_r^{(\wedge)}(x, x'')$ (see figure B1(c) for their pictorial definition). These are the probabilities of surviving two steps starting from the initial position x, jumping to a generic intermediate point x', and arriving at x''. The mid-point x' is integrated over. In the definition of $P_r^{(\vee)}(x, x'')$ the intermediate point x' has to satisfy the condition $x' > -h/4$, whereas for $P_r^{(\wedge)}(x, x'')$ one has $x' < h/4$. Formally, as it is clear from figure B1(c), the definition of $P_r^{(\vee)}(x, x'')$ is

$$P_r^{(\vee)}(x, x'') \equiv \int_0^\infty \mathrm{d}z \int_0^\infty \mathrm{d}z' \delta^{-1} \exp\Big(-\frac{z+z'}{\delta}\Big)\theta\Big(x - z + \frac{h}{4}\Big)\delta(x'' + z - z' - x). \tag{B.1}$$

In (B.1) the Heaviside theta function is to ensure the condition $x' > -h/4$. After performing the integrals, one obtains

$$P^{(\vee)}(x, x'') = \begin{cases} (2\delta)^{-1}\big(\mathrm{e}^{-|x-x''|/\delta} - \mathrm{e}^{-(h/2+x+x'')/\delta}\big) & x, x'' > -h/4 \\ 0 & \text{otherwise.} \end{cases} \tag{B.2}$$

To proceed, following the random walk literature [100], it is convenient to define $G_r^{(\vee)}(x', x, n)$ as the probability that the walker starts from position x, it survives $2n$ steps (note the factor 2), and it arrives at x''. Due to the Markovianity of the random

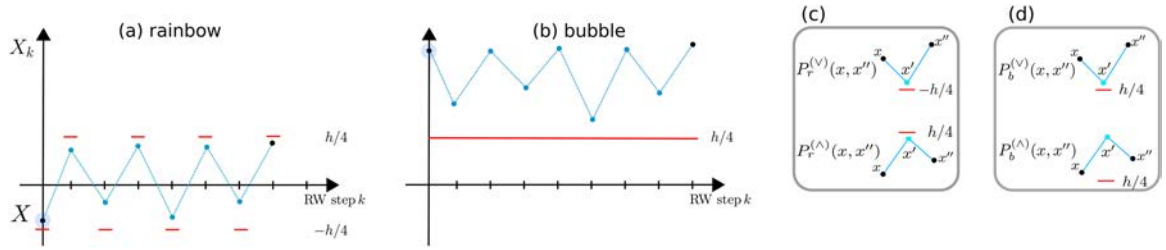

Figure B1. Random walk interpretation of the rainbow diagram (a) and of the bubble diagram (b), same as in figures 15(a) and (b). (c) The alternating random walk in (a) is constructed from the two-step survival probabilities $P_r^{(\vee)}(x,x'')$ or $P_r^{(\wedge)}(x,x'')$. The mid-point x' is integrated over in the interval $[-h/4,\infty]$. $P_r^{(\vee)}(x,x'')$ corresponds to the probability for the walker to jump from x to x'' with the condition $x' > -h/4$. (d) Similar definitions for the two-step probabilities $P_b^{(\vee)}(x,x'')$ and $P_b^{(\wedge)}(x,x'')$ for the random walk in (b).

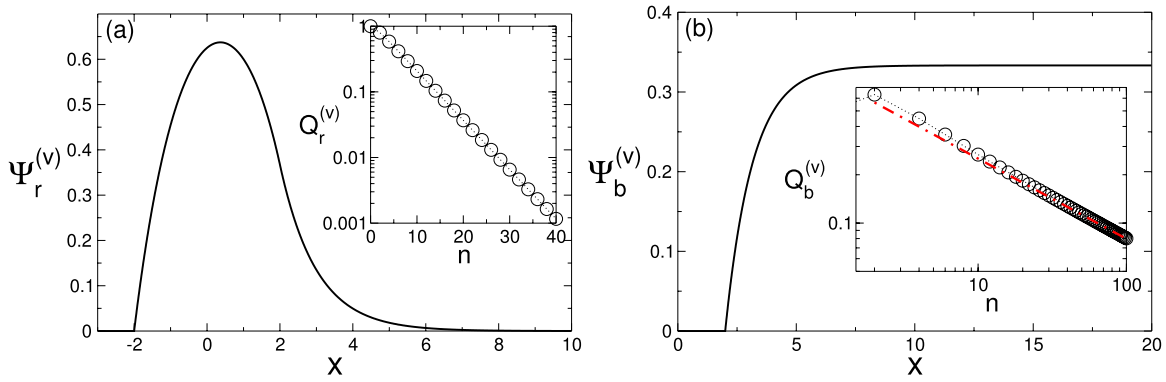

Figure B2. Generating functions $\psi_r^{(\vee)}(s,x)$ and $\psi_b^{(\vee)}(s,x)$ for the rainbow and the bubble survival probabilities. On the x-axis x is the initial point of the walker (see figure 14). The results are for fixed $s=0.5$ and $h=8$. Notice that $\psi_r^{(\vee)}$ is zero for $h<-h/4$ and it is vanishing exponentially for $x \gg h/4$. The width of the region where $\psi_r^{(\vee)}$ is significantly non-zero is $h/2$. Inset: probabilities $Q_r^{(\vee)}$ that the walker survives *at least* for n steps, plotted as a function of n. The data are for $h=8$ and $x=0$. Note the logarithmic scale on the y-axis signaling the exponential decay with n. (b) The same as in (a) for the generating function of the bubble diagrams $\psi_b^{(\vee)}$. The curve is for $h=8$ and $s=0.25$. Notice that $\psi_b^{(\vee)}$ is exactly zero for $x<h/4$ and it saturates for $x\to\infty$. This reflects that for large x the condition $X_k > h/4$ is relevant only after many steps. Inset: probabilities $Q_b^{(\vee)}$ that the walker survives for n steps plotted as a function of n. Results are for $h=8$ and $x=3$. Note the logarithmic scale on both axes, signalling a power-law behavior. The dashed-dotted line is the asymptotic result $\propto n^{-1/2}$ for large n.

walk, $G_r^{(\vee)}(x',x,n)$ has to obey the infinite system of integral equations (one for each value of n)

$$G_r^{(\vee)}(x',x,n') = \int_{-\infty}^{\frac{h}{4}} \mathrm{d}y G_r^{(\vee)}(x',y,n'-1) P_r^{(\vee)}(x,y). \tag{B.3}$$

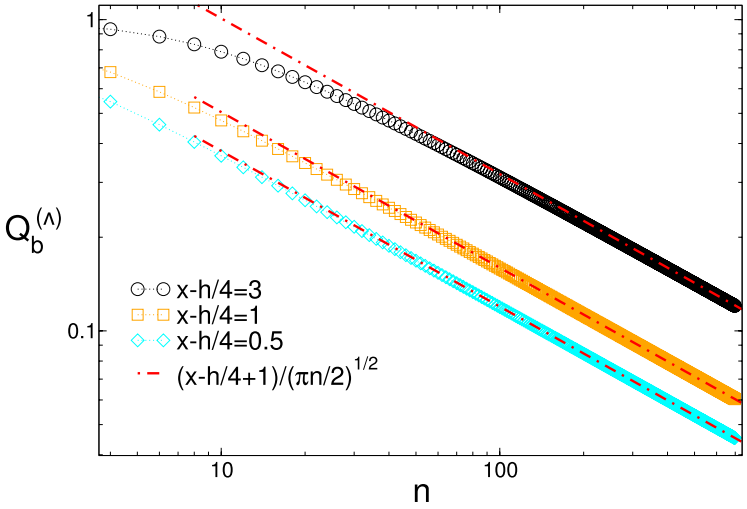

Figure B3. Survival probabilities $Q_b^{(\wedge)}$ for the bubble diagrams. Here $Q_b^{(\wedge)}(n)$ is the probability to have a bubble diagram of at least n sites. In the random walk language (see figure 15(b)) this corresponds to the probability of the walker to start from the initial point x and to stay above the line $h/4$ for at least n steps. The probabilities depend only on the combination $x - h/4$ (different symbols in the figure). Here we fixed $\delta = 1$. The dashed-dotted lines are the asymptotic results in the limit $n \to \infty$. Notice that one has $Q_b^{(\wedge)} = (x - h/4 + 1)/(\pi n/2)^{1/2}$ for $n \to \infty$.

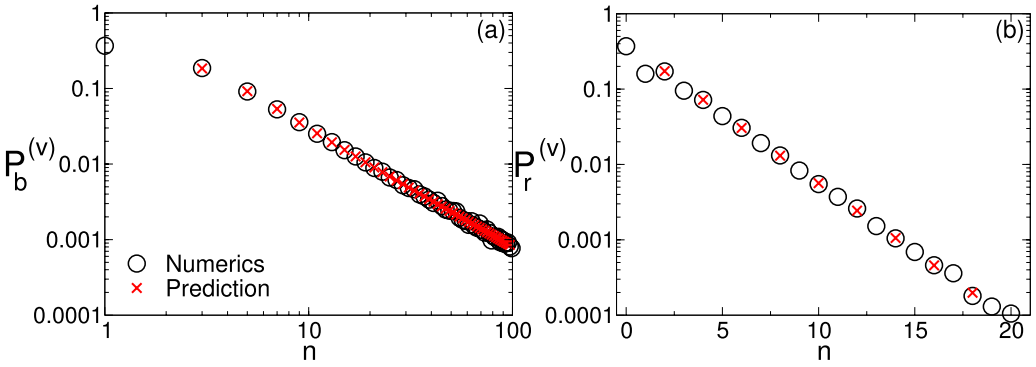

Figure B4. The alternating random walk: numerical checks. The two panels show the walker survival probabilities $P_b^{(\vee)}(n)$ and $P_r^{(\vee)}(n)$ (panels (a) and (b), respectively). Here $P_b^{(\vee)}(n)$ is defined as the probability that the walker starts from the initial point x and remains above the line $h/4$ (see figure 15) *exactly* for n steps. Notice that $P_b^{(\vee)}(2k) = 0$ for any k due to the alternation. $P_r^{(\vee)}(n)$ is the probability of the walker to start from x and stay confined in the staggered strip $[-h/4, h/4]$ (see figure 15(b)) for n steps. The circles in the panels are obtained by numerically simulating the alternating random walk and correspond to an average over ∼1000 realization of the walk. We used $x = 2$ in (a) and $x = 0$ in (b) and $h = 4$. In both panels the crosses are analytical results. In (b) only results for even n are reported.

Equation (B.3) states that the probability for the walker to survive $2n$ steps starting from position x and arriving x' is obtained from the product of the probability to jump from x to y with that of starting from y and surviving for $2n-2$ steps, by summing over all the allowed values of y.

Note that in (B.3) the integral is in $(-\infty, h/4]$, which prevents us from solving (B.3) by Fourier transform. To proceed, it is convenient to define the total survival probability $Q_r^{(\vee)}(x,n)$ by integrating over the final point of the walker as

$$Q_r^{(\vee)}(x,n) \equiv \int_{-\infty}^{\frac{h}{4}} \mathrm{d}x' G_r^{(\vee)}(x',x,n). \tag{B.4}$$

Thus, after using (B.4), equation (B.3) becomes

$$Q_r^{(\vee)}(x,n) = \int_{-\infty}^{\frac{h}{4}} \mathrm{d}y Q_r^{(\vee)}(y,n-1) P_r^{(\vee)}(x,y). \tag{B.5}$$

To solve the system of equation (B.5), it is convenient to define the generating function $\psi_r^{(\vee)}(x,s)$ as

$$\psi_r^{(\vee)}(x,s) \equiv \sum_{m=1}^{\infty} Q_r^{(\vee)}(x,m) s^m, \tag{B.6}$$

where s is a real parameter. The probabilities $Q_r^{(\vee)}(x,n)$ are obtained as the coefficients of the Taylor expansion of $\psi_r^{(\vee)}(x,s)$ around $s=0$. After substituting (B.6) in (B.5) one obtains the integral equation

$$\psi_r^{(\vee)}(x,s) = s \int_{-\infty}^{\frac{h}{4}} \mathrm{d}x' \psi_r^{(\vee)}(x',s) P_r^{(\vee)}(x,x') + s \int_{-\infty}^{\frac{h}{4}} \mathrm{d}x' P_r^{(\vee)}(x,x'). \tag{B.7}$$

For generic distributions $P_r^{(\vee)}(x,x')$ it is difficult to solve (B.7) analytically. However, for the exponential distribution in (B.2) the solution of (B.7) is straightforward. The key ingredient is the identity

$$\left[P_r^{(\vee)}(x,x')\right]'' = \frac{1}{\delta^2}\left[P_r^{(\vee)}(x,x') - \delta(x-x')\right] \quad \text{with } [\,f(x)]'' \equiv \frac{\mathrm{d}^2 f}{\mathrm{d}x^2}. \tag{B.8}$$

Thus, after taking the second derivative with respect to x in (B.7), and after using (B.8), one obtains a linear system of differential equations as

$$\begin{cases} \delta^2\left[\psi_r^{(\vee)}\right]'' = (1-s)\psi_r^{(\vee)} - s & -h/4 \leqslant x \leqslant h/4 \\ \delta^2\left[\psi_r^{(\vee)}(x,s)\right]'' = \psi_r^{(\vee)} & x > h/4 \\ \psi_r^{(\vee)} = 0 & x < -h/4. \end{cases} \tag{B.9}$$

The solution of (B.9) is straightforward. First, one solves independently (B.9) in the three independent domains $(-\infty, -h/4]$, $(-h/4, h/4]$, and $(h/4, \infty)$. After discarding the divergent solutions for $x \to \pm\infty$, one has to match the different solutions by imposing the continuity of $\psi_r^{(\vee)}$ at $x = \pm h/4$ and of its first derivative $[\psi_r^{(\vee)}]'$ at $x = h/4$. Eventually, one obtains for $-h/4 \leqslant x \leqslant h/4$

$$\psi_r^{(\vee)}(x,s) = \frac{s}{1-s} + \frac{s\mathrm{e}^{\sqrt{1-s}h/(4\delta)}}{(-1+\mathrm{e}^{\sqrt{1-s}h/\delta}+\sqrt{1-s}+\mathrm{e}^{\sqrt{1-s}h/\delta}\sqrt{1-s})(s-1)}$$
$$\times\left[(\mathrm{e}^{\sqrt{1-s}h/(2\delta)}+\sqrt{1-s}-1)\mathrm{e}^{\sqrt{1-s}x/\delta}+(\mathrm{e}^{\sqrt{1-s}h/(2\delta)}+\mathrm{e}^{\sqrt{1-s}h/(2\delta)}\sqrt{1-s}-1)\mathrm{e}^{-\sqrt{1-s}x/\delta}\right]. \tag{B.10}$$

On the other hand, for $x > h/4$, one obtains

$$\psi_r^{(\vee)}(x,s) = -\frac{s\mathrm{e}^{h/(4\delta)}(-1+\mathrm{e}^{\sqrt{1-s}h/(2\delta)})^2\sqrt{1-s}\mathrm{e}^{-\sqrt{1-s}x/\delta}}{(-1+\mathrm{e}^{\sqrt{1-s}h/\delta}+\mathrm{e}^{\sqrt{1-s}h/\delta}\sqrt{1-s})(s-1)}. \tag{B.11}$$

Importantly, the generating function, and therefore the probabilities $Q_r^{(\vee)}$, depend only on h/δ and x/δ. This also reflects that the von Neumann entropy is a function of the ratio h/δ. For completeness we now discuss the result for $\psi_r^{(\wedge)}(x,s)$. The probability $P_r^{(\wedge)}(x,x'')$ (see figure 15(c)) is now given as

$$P_r^{(\wedge)}(x,x'') = \begin{cases} (2\delta)^{-1}\left(\mathrm{e}^{-|x-x''|/\delta} - \mathrm{e}^{(-h/2+x+x'')/\delta}\right) & x,x'' < h/4 \\ 0 & \text{otherwise.} \end{cases} \tag{B.12}$$

By comparing (B.2) and (B.12), one has that $P_r^{(\wedge)}(x,x'') = P_r^{(\vee)}(-x,-x'')$. One now has to solve the integral equation (the analog of (B.7))

$$\psi_r^{(\wedge)}(x,s) = s\int_{-\frac{h}{4}}^{\infty} \mathrm{d}x'\psi_r^{(\wedge)}(x',s)P_r^{(\wedge)}(x,x') + s\int_{-\frac{h}{4}}^{\infty} \mathrm{d}x' P_r^{(\wedge)}(x,x'). \tag{B.13}$$

It is trivial to show that equation (B.13) is obtained from (B.7) after the change of variables $x \to -x$. Clearly, this implies that

$$\psi_r^{(\wedge)}(x,s) = \psi_r^{(\vee)}(-x,s). \tag{B.14}$$

Finally, we should stress that the nth order coefficient of the Taylor series of the generating function $\psi_r^{(\wedge)}$ around $s=0$ is the probabilities $Q_r^{(\wedge)}$ of the walker to survives for at least $2n$ steps within the alternating strip in figure 15(a). The generating function $\psi_r^{(\mathrm{odd})}$ for the probability for the walker to survive an odd number of steps $2n+1$ is obtained from $\psi_r^{(\wedge)}$ by performing an extra integration. Formally, one has

$$\psi_r^{(\mathrm{odd})}(x,s) = \int_{-\frac{h}{4}}^{\frac{h}{4}} \mathrm{d}x'\delta^{-1}\mathrm{e}^{-|x-x'|/\delta}\psi_r^{(\wedge)}(x',s)\theta(x-x'), \quad \text{for } x < \frac{h}{4} \tag{B.15}$$

whereas, $\psi_r^{(\mathrm{odd})}(x,s) = 0$ for $x > h/4$. The survival proability for odd number of steps $Q_r(x,2n+1)$ corresponds to the nth coefficient in the series expansion of $\psi_r^{(\mathrm{odd})}(x,s)$ around $s=0$.

It is interesting to investigate the behavior of $\psi_r^{(\vee)}$ as a function of the initial point of the walker x. This is shown in figure B2(a) for fixed $s=0.5$, $h=8$, and $\delta=1$. $\psi_r^{(\vee)}$ is zero for $x < -h/4$ and it is vanishing exponentially for $x \to \infty$. Similar behavior is found for different values of s. The inset in the figure shows the probability $Q_r^{(\vee)}$ for the walker to survive n steps, as a function of n. Clearly, it decays exponentially (note the logarithmic scale on the y-axis).

B.2. Bubble diagram

We now derive analytically the probability for the walker to remain above the line $h/4$ (see figure B1(b)). As in the previous section, we can define the generating function $\psi_b^{(\vee)}(x,s)$ for the probability to survive an even number of steps n. The building block two-steps probability $P_b^{(\vee)}(x,x'')$ is defined in figure B1(d), and it is given as

$$P_s^{(\vee)}(x,x'') = \begin{cases} (2\delta)^{-1}\left(\mathrm{e}^{-|x-x''|/\delta} - \mathrm{e}^{(h/2-x-x'')/\delta}\right) & x,x'' > h/4 \\ 0 & \text{otherwise.} \end{cases} \tag{B.16}$$

Notice that $P_b^{(\vee)}$ is obtained from $P_r^{(\vee)}$ after sending $h \to -h$, as it clear from comparing figures B1(c) and (d). The equation for $\psi_b^{(\vee)}(x,s)$ reads

$$\psi_b^{(\vee)}(x,s) = s\int_{\frac{h}{4}}^{\infty} \mathrm{d}x' P_b^{(\vee)}(x,x')\psi_s^{(\vee)}(x',s) + s\int_{\frac{h}{4}}^{\infty} \mathrm{d}x' P_b^{(\vee)}(x,x'). \tag{B.17}$$

As in the previous section, equation (B.17) can be reduced to a system of differential equations. Specifically, $\psi_b^{(\vee)}$ is obtained by solving the system

$$\begin{cases} \psi_b^{(\vee)}(x,s) = 0 & x \leqslant h/4 \\ \delta^2[\psi_b^{(\vee)}]'' = (1-s)\psi_b^{(\vee)} - s & x > h/4. \end{cases} \tag{B.18}$$

In contrast with equation (B.9), the domain of the system (B.18) is composed of the two half-infinite intervals $(-\infty, h/4]$ and $[h/4, \infty)$. The solution for $x > h/4$ is given as

$$\psi_b^{(\vee)} = -\frac{s}{1-s}\mathrm{e}^{-\sqrt{1-s}(x-h/4)/\delta} + \frac{s}{1-s}. \tag{B.19}$$

The strategy to derive the generating function $\psi_b^{(\wedge)}$ is similar, and we do not report the calculation, quoting only the final result. One obtains

$$\psi_b^{(\wedge)} = \frac{s}{1-s} + \frac{s\mathrm{e}^{\sqrt{1-s}(h/4-x)/\delta}}{(1+\sqrt{1-s})(s-1)}, \quad \text{for } x > h/4 \tag{B.20}$$

$$\psi_b^{(\wedge)} = \frac{s\mathrm{e}^{(-h/4+x)/\delta}}{(1+\sqrt{1-s})\sqrt{1-s}}, \quad \text{for } x \leqslant h/4. \tag{B.21}$$

In the limit $x \to \infty$ one has $\psi_b^{(\wedge)} = s/(1-s)$. This reflects that if the starting point of the walker is at $x \to \infty$, it remains above the line $h/4$ for an infinite number of steps.

The probability $Q_b^{(\wedge)}$ that the walker survives for at least $2n$ steps is the nth coefficient of the Taylor expansion of $\psi_b^{(\wedge)}$ around $s = 0$. Notice that for the bubble diagram, the probability that the walker survives at least for $2n+1$ steps is the same as that for surviving $2n$ steps. This is clear from figure B2(b), and it is due to the fact that the random walk is alternating.

We now discuss the structure of $\psi_b^{(\vee)}$. A similar behavior is observed for $\psi_b^{(\wedge)}$. The result is shown in figure B2(b). The data are for $h = 8$ and $s = 0.25$. Clearly, the generating function vanishes for $x < h/4$, while it saturates to $s/(1-s)$ in the limit $x \to \infty$. The inset in the figure shows the survival probabilities $Q_b^{(\vee)}(x,n)$ for the walker to start

from x and survive for at least n steps. In contrast with the survival probability for the rainbow, which decays exponentially (see figure B2(a)), now the decay for large n is power law as

$$Q_b^{(\vee)}(x,n) \propto n^{-\frac{1}{2}}. \tag{B.22}$$

Using equation (B.22) it is straightforward to derive the probability $P_b^{(\vee)}$ that the walker survives *exactly* n steps as

$$P_b^{(\vee)} \equiv Q_b^{(\vee)}(n) - Q_b^{(\vee)}(n+1). \tag{B.23}$$

Since $Q_b^{(\vee)}(n+1) = Q_b^{(\vee)}(n)$ for any n odd, one has that $P_b^{(\vee)}(n) = 0$ for any n odd. Oppositely, one has that $P_b^{(\wedge)}(n) = 0$ for n even. Finally, using (B.22), one has that $P_b^{(\vee)}$ (and $P_b^{(\wedge)}$) for large n decays as

$$P_b^{(\vee)}(n) \equiv Q_b^{(\vee)}(x,n) - Q_b^{(\vee)}(x,n+1) \propto n^{-\frac{3}{2}}. \tag{B.24}$$

B.3. Asymptotic behavior of the length of the bubble diagrams

The asymptotic behavior as $n^{-1/2}$ of $Q_b^{(\wedge)}(x,n)$ (and of $Q_b^{(\wedge)}$) can be obtained analytically by studying the coefficients of the Taylor series of $\psi_s^{(\wedge)}(x,s)$ around $s=0$. Here we focus on the generating function for $x > h/4$. First, it is convenient to rewrite the generating function (B.20) as

$$\psi_b^{(\wedge)}(x,s) = \frac{s}{1-s} - s\mathrm{e}^{\sqrt{1-s}(h/4-x)/\delta}\left[\frac{1}{1+(1-s)^{\frac{1}{2}}} + \frac{1}{1-s} - \frac{1}{(1-s)^{\frac{1}{2}}}\right]. \tag{B.25}$$

One can check that the first term in the square brackets in (B.25) gives a subleading contribution in the limit $n \to \infty$, and it can be neglected. Now we focus on the second term in the brackets. It is useful to observe that

$$\frac{\mathrm{e}^{-a\sqrt{1-s}}}{1-s} = -a\sum_{k=0}^{\infty}\frac{a^{2k}(1-s)^{k-1/2}}{(2k+1)!} + \sum_{k=0}^{\infty}\frac{a^{2k}(1-s)^{k-1}}{(2k)!}, \quad \text{with } a \equiv \frac{1}{\delta}\Big(x - \frac{h}{4}\Big). \tag{B.26}$$

The first term in (B.26) can be rewritten as

$$-a\sum_{k=0}^{\infty}\frac{a^{2k}(1-s)^{k-1/2}}{(2k+1)!} \equiv \sum_{n=0} c_n s^n, \quad \text{with } c_n \equiv -\sum_{k=0}^{\infty}\frac{a^{2k+1}\Gamma(n-k+1/2)}{\Gamma(-k+1/2)\Gamma(n+1)\Gamma(2k+2)}. \tag{B.27}$$

Here we are interested in the limit $n \to \infty$ of c_n. In this limit one can expand the terms $\Gamma(n-k+1/2)$ and $\Gamma(n+1)$ in (B.27) to obtain

$$c_n \to -\sum_{k=0}^{\infty}\frac{a^{2k+1}n^{-k-1/2}}{\Gamma(-k+1/2)\Gamma(2k+2)} = -\mathrm{Erf}\Big(\frac{a}{2\sqrt{n}}\Big) \to -\frac{a}{\sqrt{\pi n}}. \tag{B.28}$$

In the last step in (B.28) we used the expansion of the error function $\mathrm{Erf}(x)$ around $x=0$. On the other hand, the second sum in (B.26) gives

$$\sum_{k=0}^{\infty}\frac{a^{2k}(1-s)^{k-1}}{(2k)!} \equiv \sum_{n=0}^{\infty} c'_n s^n, \quad \text{with } c'_n \equiv \sum_{k=0}^{\infty}\frac{a^{2k}\Gamma(n-k+1)}{\Gamma(-k+1)\Gamma(n+1)\Gamma(2k+1)}. \tag{B.29}$$

The factor $\Gamma(-k+1)$ implies that only the term with $k=0$ is nonzero. The result cancels out with the term $s/(1-s)$ in (B.25).

A similar analysis can be performed for the last term in (B.25). One obtains

$$\frac{s\mathrm{e}^{-a\sqrt{1-s}}}{(1-s)^{\frac{1}{2}}} \equiv \sum_{n=0}^{\infty} c''_n s^n, \quad \text{with } c''_n \to \frac{1}{\sqrt{\pi n}}. \tag{B.30}$$

Notice that the right hand side in (B.30) does not depend on a. The asymptotic behavior of $Q_b^{(\vee)}$ for large n is obtained by putting together (B.30) and (B.28). A similar approach can be used to derive the asymptotic behavior of $Q_b^{(\vee)}(x,n)$. Our final formulas read

$$Q_b^{(\wedge)}(x,n) \propto \left(x - \frac{h}{4} + 1\right)\frac{\sqrt{2}}{\delta\sqrt{\pi n}}, \qquad Q_b^{(\vee)}(x,n) \propto \left(x - \frac{h}{4}\right)\frac{\sqrt{2}}{\delta\sqrt{\pi n}}. \tag{B.31}$$

The factor $\sqrt{2}$ in (B.31) takes into account that the nth order coefficient in the expansion of the generating functions around $s=0$ is the probability of surviving at least $2n$ steps.

Finally, we provide some numerical checks of the validity of (B.31). The results are reported in figure B3 for $Q_b^{(\wedge)}(x,n)$. The figure shows $Q_b^{(\wedge)}(x,n)$ versus n. The different symbols correspond to different values of $x - h/4$. The dashed-dotted lines are the asymptotic results obtained from (B.31), and they perfectly describe the numerical data.

Appendix C. Random walk survival probabilities: numerical simulations

In this section we provide some numerical checks of the analytical results for the walker survival probabilities $P_r^{(\vee)}(n)$ and $P_b^{(\vee)}(n)$. The former is the probability that the alternating random walk is confined in the strip $[-h/4, h/4]$ (see figure B1(a)) for exactly n steps, whereas the latter is the probability that the walk remains above the line $h/4$ for exactly n steps (see figure B1(b)). The analytical results for the probabilities are obtained as

$$P_b^{(\vee)}(n) = Q_b^{(\vee)}(n) - Q_b^{(\vee)}(n+1), \tag{C.1}$$

$$P_r^{(\vee)}(n) = Q_r^{(\vee)}(n) - Q_r^{(\vee)}(n+1), \tag{C.2}$$

where $Q_b^{(\vee)}$ and $Q_r^{(\vee)}$ are obtained from the generating functions $\psi_b^{(\vee)}$ and $\psi_r^{(\vee)}$. To benchmark equation (C.1) here we present numerical data obtained by simulating directly the alternating random walk (see (18)) that describes the SDRG flow of the couplings. Our results are shown in figure B4. Panel (a) shows $P_b^{(\vee)}(n)$ plotted as function of n. The data are for fixed $h=4$ and initial point of the walker $x=h/4$. The data are averaged over $\sim$1000 realizations of the random walk. Notice that, due to the alternating structure (see figure B1), one has that $P_b^{(\vee)}(2n)=0$, as it is clear from figure B1(b). The crosses figure B4 are the theoretical predictions using (C.2). Panel (b) in the figure focuses on the random walk in figure B1(a). For simplicity we focus on the case with $h=4$ and $x=0$. The survival probabailities decay exponentially with n (note the

logarithmic scale on the y-axis). The crosses are now the theory predictions calculated from (C.1). We only show results for even n, although $P_r(n)$ for n odd is nonzero. Clearly, the analytical results are in perfect agreement with the numerical data.

References

[1] Eisert J, Cramer M and Plenio M B 2010 Colloquium: Area law for the entanglement entropy *Rev. Mod. Phys.* **82** 277

[2] Amico L, Fazio R, Osterloh A and Vedral V 2008 Entanglement in many-body systems *Rev. Mod. Phys.* **80** 517

[3] Calabrese P, Cardy J and Doyon B 2009 Entanglement entropy in extended quantum systems *J. Phys. A: Math. Theor.* **42** 500301

[4] Laflorencie N 2016 Quantum entanglement in condensed matter systems *Phys. Rep.* **646** 1

[5] White S R 1992 Density matrix formulation for quantum renormalization groups *Phys. Rev. Lett.* **69** 2863

[6] White S R 1993 Density-matrix algorithms for quantum renormalization groups *Phys. Rev.* B **48** 10345

[7] Schollwöck U 2011 The density-matrix renormalization group in the age of matrix product states *Ann. Phys.* **326** 96

[8] Hastings M B 2007 An area law for one dimensional quantum systems *J. Stat. Mech.* P08024

[9] Arad I, Kitaev A, Landau Z and Vazirani U 2013 An area law and sub-exponential algorithm for 1D systems (arXiv:1301.1162)

[10] Wolf M M 2006 Violation of the entropic area law for Fermions *Phys. Rev. Lett.* **96** 010404

[11] Gioev D and Klich I 2006 Entanglement entropy of fermions in any dimension and the widom conjecture *Phys. Rev. Lett.* **96** 100503

[12] Calabrese P, Mintchev M and Vicari E 2012 Entanglement entropies in free fermion gases for arbitrary dimension *Europhys. Lett.* **97** 20009

[13] Plenio M B, Eisert J, Dreißig J and Cramer M 2005 Entropy, entanglement, and area: analytical results for harmonic lattice systems *Phys. Rev. Lett.* **94** 060503

[14] Holzhey C, Larsen F and Wilczek F 1994 Geometric and renormalized entropy in conformal field theory *Nucl. Phys.* B **424** 443

[15] Calabrese P and Cardy J 2004 Entanglement entropy and quantum field theory *J. Stat. Mech.* P06002

[16] Vidal G, Latorre J I, Rico E and Kitaev A 2003 Entanglement in quantum critical phenomena *Phys. Rev. Lett.* **90** 227902

[17] Calabrese P and Cardy J 2009 Entanglement entropy and conformal field theory *J. Phys. A: Math. Theor.* **42** 504005

[18] Popkov V and Salerno M 2005 Logarithmic divergence of the block entanglement entropy for the ferromagnetic Heisenberg model *Phys. Rev.* A **71** 012301

[19] Ercolessi E, Evangelisti S, Franchini F and Ravanini F 2011 Essential singularity in the Renyi entanglement entropy of the one-dimensional XYZ spin-1/2 chain *Phys. Rev.* B **83** 012402

[20] Alba V, Haque M and Läuchli A M 2012 Entanglement spectrum of the Heisenberg XXZ chain near the ferromagnetic point *J. Stat. Mech.* P08011

[21] Castro-Alvaredo O A and Doyon B 2012 Entanglement entropy of highly degenerate states and fractal dimensions *Phys. Rev. Lett.* **108** 120401

[22] Goldstein S, Lebowitz J L, Tumulka R and Zanghi N 2006 Canonical typicality *Phys. Rev. Lett.* **96** 050403

[23] Hayden P, Leung D W and Winter A 2006 Aspects of generic entanglement *Commun. Math. Phys.* **265** 95

[24] Alba V, Fagotti M and Calabrese P 2009 Entanglement entropy of excited states *J. Stat. Mech.* P10020

[25] Alba V and Calabrese P 2017 Entanglement and thermodynamics after a quantum quench in integrable systems *Proc. Natl Acad. Sci.* **114** 7947

Alba V and Calabrese P 2018 Entanglement dynamics after quantum quenches in generic integrable systems *SciPost Phys.* **4** 017

[26] Castro-Alvaredo O A, De Fazio C, Doyon B and Szecsenyi I M 2018 Entanglement content of quasi-particle excitations (arXiv:1805.04948)

Castro-Alvaredo O A, De Fazio C, Doyon B and Szecsenyi I M 2018 Entanglement content of quantum particle excitations I. Free field theory (arXiv:1806.03247)

[27] Alcaraz F C, Ibanez Berganza M and Sierra G 2011 Entanglement of low-energy excitations in conformal field theory *Phys. Rev. Lett.* **106** 201601

[28] Ibanez Berganza M, Alcaraz F C and Sierra G 2012 Entanglement of excited states in critical spin chains *J. Stat. Mech.* P01016

[29] Palmai T 2014 Excited state entanglement in one dimensional quantum critical systems: extensivity and the role of microscopic details *Phys. Rev.* B **90** 161404
[30] Palmai T 2016 Entanglement entropy from the truncated conformal space *Phys. Lett.* B **759** 439
[31] Taddia L, Xavier J C, Alcaraz F C and Sierra G 2013 Entanglement entropies in Conformal Systems with Boundaries *Phys. Rev.* B **88** 075112
[32] Taddia L, Ortolani F and Palmai T 2016 Renyi entanglement entropies of descendant states in critical systems with boundaries: conformal field theory and spin chains *J. Stat. Mech.* 093104
[33] Essler F H L, Läuchli A M and Calabrese P 2013 Shell-filling effect in the entanglement entropies of spinful fermions *Phys. Rev. Lett.* **110** 115701
[34] Calabrese P, Essler F and Läuchli A 2014 Entanglement entropies of the quarter filled Hubbard model *J. Stat. Mech.* P09025
[35] Calabrese P, Mintchev M and Vicari E 2011 The entanglement entropy of 1D systems in continuous and homogenous space *J. Stat. Mech.* P09028
[36] Farkas S and Zimboras Z 2005 On the sharpness of the zero-entropy-density conjecture *J. Math. Phys.* **46** 123301
[37] Irani S 2010 Ground state entanglement in one dimensional translationally invariant quantum systems *J. Math. Phys.* **51** 022101
[38] Gottesman D and Hastings M B 2010 Entanglement versus gap for one-dimensional spin systems *New J. Phys.* **12** 025002
[39] Vitagliano G, Riera A and Latorre J I 2010 Volume-law scaling for the entanglement entropy in spin-1/2 chains *New J. Phys.* **12** 113049
[40] Bravyi S, Caha L, Movassagh R, Nagaj D and Shor P W 2012 Criticality without frustration for quantum spin-1 chains *Phys. Rev. Lett.* **109** 207202
[41] Huijse L and Swingle B 2013 Area law violations in a supersymmetric model *Phys. Rev.* B **87** 035108
[42] Shiba N and Takayanagi T 2014 Volume law for the entanglement entropy in non-local QFTs *J. High Energy Phys.* JHEP02(2014)033
[43] Gori G, Paganelli S, Sharma A, Sodano P and Trombettoni A 2015 Explicit Hamiltonians inducing volume law for entanglement entropy in fermionic lattices *Phys. Rev.* B **91** 245138
[44] Movassagh R and Shor P W 2016 Supercritical entanglement in local systems: counterexample to the area law for quantum matter *Proc. Natl Acad. Sci.* **113** 13278
[45] Dell'Anna L, Salberger O, Barbiero L, Trombettoni A and Korepin V E 2016 Violation of cluster decomposition and absence of light cones in local integer and half-integer spin chains *Phys. Rev.* B **94** 155140
[46] Salberger O and Korepin V 2016 Fredkin spin chains (arXiv:1605.03842)
[47] Zhang Z, Ahmadain A and Klich I 2017 Novel quantum phase transition from bounded to extensive entanglement *Proc. Natl Acad. Sci.* **114** 5142
[48] Salberger O, Udagawa T, Zhang Z, Katsura H, Klich I and Korepin V E 2017 Deformed Fredkin spin chain with extensive entanglement *J. Stat. Mech.* 063103
[49] Sugino F and Padmanabhan P 2018 Area law violations and quantum phase transitions in modified Motzkin walk spin chains *J. Stat. Mech.* 013101
[50] Caha L and Nagaj D 2018 The pair-flip model: a very entangled translationally invariant spin chain (arXiv:1805.07168)
[51] Sugino F and Korepin V 2018 Renyi entropy of highly entangled spin chains *Int. J. Mod. Phys.* B **32** 1850306
[52] Motzkin T 1948 Relations between hypersurface cross ratios, and a combinatorial formula for partitions of a polygon, for permanent preponderance, and for nonassociative products *Bull. Am. Math. Soc.* **54** 352
[53] Fredkin E and Toffoli T 1982 Conservative logic *Int. J. Theor. Phys.* **21** 219
[54] Iglói F and Monthus C 2005 Strong disorder RG approach of random systems *Phys. Rep.* **412** 277–431
[55] Iglói F and Monthus C 2018 Strong Disorder RG approach—a short review of recent developments *Eur. Phys. J.* B **91** 290
[56] Dasgupta C and Ma S-K 1980 Low-temperature properties of the random Heisenberg antiferromagnetic chain *Phys. Rev.* B **22** 1305
[57] Fisher D S 1995 Critical behavior of random transverse-field Ising spin chains *Phys. Rev.* B **51** 6411
[58] Refael G and Moore J E 2004 Entanglement entropy of random quantum critical points in one dimension *Phys. Rev. Lett.* **93** 260602
[59] Refael G and Moore J E 2009 Criticality and entanglement in random quantum systems *J. Phys. A: Math. Theor.* **42** 504010
[60] Laflorencie N 2005 Scaling of entanglement entropy in the random singlet phase *Phys. Rev.* B **72** 140408
[61] Fagotti M, Calabrese P and Moore J E 2011 Entanglement spectrum of random-singlet quantum critical points *Phys. Rev.* B **83** 045110

[62] Santachiara R 2006 Increasing of entanglement entropy from pure to random quantum critical chains *J. Stat. Mech.* L06002
[63] Ramírez G, Rodríguez-Laguna J and Sierra G 2014 From conformal to volume law for the entanglement entropy in exponentially deformed critical spin 1/2 chains *J. Stat. Mech.* P10004
[64] Ramírez G, Rodríguez-Laguna J and Sierra G 2015 Entanglement over the rainbow *J. Stat. Mech.* P06002
[65] Ramírez G, Rodríguez-Laguna J and Sierra G 2014 Entanglement in low-energy states of the random-hopping model *J. Stat. Mech.* P07003
[66] Rodriguez-Laguna J, Santalla S N, Ramirez G and Sierra G 2016 Entanglement in correlated random spin chains, RNA folding and kinetic roughening *New J. Phys.* **18** 073025
[67] Rodriguez-Laguna J, Dubail J, Ramirez G, Calabrese P and Sierra G 2017 More on the rainbow chain: entanglement, space-time geometry and thermal states *J. Phys. A: Math. Theor.* **50** 164001
[68] Lin Y-C, Igloi F and Rieger H 2007 Entanglement entropy at infinite randomness fixed points in higher dimensions *Phys. Rev. Lett.* **99** 147202
[69] Iglói F, Szatmari Z and Lin Y-C 2012 Entanglement entropy dynamics of disordered quantum spin chains *Phys. Rev.* B **85** 094417
[70] Hoyos J A, Vieira A P, Laflorencie N and Miranda E 2007 Correlation amplitude and entanglement entropy in random spin chains *Phys. Rev.* B **76** 174425
[71] Juhász R and Zimborás Z 2007 Entanglement entropy in aperiodic singlet phases *J. Stat. Mech.* P04004
[72] Iglói F, Juhász R and Zimborás Z 2009 Entanglement entropy of aperiodic quantum spin chains *Eur. Phys. Lett.* **79** 37001
Iglói F and Lin Y-C 2008 Finite-size scaling of the entanglement entropy of the quantum Ising chain with homogeneous, periodically modulated and random couplings *J. Stat. Mech.* P06004
[73] Hoyos J A, Laflorencie N, Vieira A P and and Vojta T 2011 Protecting clean critical points by local disorder correlations *Eur. Phys. Lett.* **93** 30004
[74] Kovács I A and Iglói F 2012 Universal logarithmic terms in the entanglement entropy of 2d, 3d and 4d random transverse-field Ising models *Europhys. Lett.* **97** 67009
[75] Vosk R and Altman E 2013 Many-body localization in one dimension as a dynamical renormalization group fixed point *Phys. Rev. Lett.* **110** 067204
[76] Juhász R, Kovács I A and Iglói F 2014 Random transverse-field Ising chain with long-range interactions *Europhys. Lett.* **107** 47008
[77] Getelina J C, Alcaraz F C and Hoyos J A 2016 Entanglement properties of correlated random spin chains and similarities with conformally invariant systems *Phys. Rev.* B **93** 045136
[78] Ruggiero P, Alba V and Calabrese P 2016 The entanglement negativity in random spin chains *Phys. Rev.* B **94** 035152
[79] Juhász R, Kovács I A, Roósz G and Iglói F 2017 Entanglement between random and clean quantum spin chains *J. Phys. A: Math. Theor.* **50** 324003
[80] Juhász R 2017 Entanglement across extended random defects in the XX spin chain *J. Stat. Mech.* 083107
[81] Chen Y and Vidal G 2014 Entanglement contour *J. Stat. Mech.* P10011
[82] Alba V, Haque M and Läuchli A M 2012 Boundary-locality and perturbative structure of entanglement spectra in gapped systems *Phys. Rev. Lett.* **108** 227201
[83] Alba V, Haque M and Läuchli A M 2013 Entanglement spectrum of the two dimensional Bose–Hubbard model *Phys. Rev. Lett.* **110** 260403
[84] Coser A, De Nobili C and Tonni E 2017 A contour for the entanglement entropies in harmonic lattices *J. Phys. A: Math. Theor.* **50** 314001
[85] Frerot I and Roscilde T 2015 Area law and its violation: a microscopic inspection into the structure of entanglement and fluctuations *Phys. Rev.* B **92** 115129
[86] Tonni E, Rodríguez-Laguna J and Sierra G 2018 Entanglement Hamiltonian and entanglement contour in inhomogeneous 1D critical systems *J. Stat. Mech.* 043105
[87] Peschel I, Kaulke M and Legeza O 1999 Density matrix spectra for integrable models *Ann. Phys., Lpz.* **8** 153
[88] Peschel I and Chung M-C 1999 Density matrices for a chain of oscillators *J. Phys. A: Math. Gen.* **32** 8419
[89] Chung M-C and Peschel I 2001 Density-matrix spectra of solvable fermionic systems *Phys. Rev.* B **64** 064412
[90] Peschel I 2003 Calculation of reduced density matrices from correlation functions *J. Phys. A: Math. Gen.* **36** L205
[91] Peschel I 2004 On the reduced density matrix for a chain of free electrons *J. Stat. Mech.* P06004
[92] Peschel I and Eisler V 2009 Reduced density matrices and entanglement entropy in free lattice models *J. Phys. A: Math. Theor.* **42** 504003
[93] Levine L and Movassagh R 2017 The gap of the area-weighted Motzkin spin chain is exponentially small *J. Phys. A: Math. Theor.* **50** 255302

[94] Movassagh R 2018 The gap of Fredkin quantum spin chain is polynomially small *Ann. Math. Sci. Appl.* **3** 531
[95] Udagawa T and Katsura H 2017 Finite-size gap, magnetization, and entanglement of deformed Fredkin spin chain *J. Phys. A: Math. Theor.* **50** 405002
[96] Dubail J, Stéphan J-M, Viti J and Calabrese P 2017 Conformal field theory for inhomogeneous one-dimensional quantum systems: the example of non-interacting Fermi gases *SciPost Phys.* **2** 002
[97] Calabrese P and Cardy J 2005 Evolution of entanglement entropy in one-dimensional systems *J. Stat. Mech.* P04010
[98] Calabrese P and Cardy J 2007 Entanglement and correlation functions following a local quench: a conformal field theory approach *J. Stat. Mech.* P10004
[99] Bazunova N, Borowiec A and Kerner R 2004 Universal differential calculus on ternary algebras *Lett. Math. Phys.* **67** 195
[100] Majumdar S N 2010 Universal first-passage properties of discrete-time random walks and Levy flights on a line: statistics of the global maximum and records *Physica* A **389** 4299
[101] Comtet A and Majumdar S N 2005 Precise asymptotics for a random Walker's maximum *J. Stat. Mech.* P06013